SHEAR LAG OF BOLTED AND WELDED SINGLE ANGLES WITH HIGH STRENGTH STEELS

XIONG YUHAO

M.Phil

The Hong Kong Polytechnic University

2017

The Hong Kong Polytechnic University

Department of Building and Real Estate

Shear Lag of Bolted and Welded Single Angles with High Strength Steels

Xiong Yuhao

A thesis submitted in partial fulfilment of

the requirements for the degree of

Master of Philosophy

May 2016

CERTIFICATE OF ORIGINALITY

I hereby declare that this thesis is my own work and that, to the best of my knowledge and belief, it reproduces no material previously published or written, nor material that has been accepted for the award of any other degree or diploma, except where due acknowledgement has been made in the text.

XIONG YUHAO

ABSTRACT

High strength steels (HSS) have been attracting increasing attention in the design and construction industry because of their high ultimate strength and reduced cost of production. With the increased ultimate strength, smaller HSS structural sections can be designed and used in structural systems. This scenario translates to weight reduction and cost saving. However, HSS possess lower ductility than normal steels (NS), thereby possibly affecting the structural behaviour of members and connections. In particular, the reduced ductility of steel materials may have a significant influence on the tensile strength and behaviour of angle sections, which are usually governed by the shear lag effect. The current design equations used to evaluate the tensile capacity of angle sections considering the shear lag effect are based on studies using NS materials, and the existing literature on HSS tension member strength and behaviour is scarce. Therefore, a study including both experimental and numerical works was conducted to examine the tensile strength and the behaviour of HSS angle sections. A total of 18 full-scale bolted and welded single angles were tested, including 14 HSS angle specimens and 4 NS angle specimens. The test parameters included steel grade, connection length and out-of-plane eccentricity. Finite element models were established and validated using test results, and a numerical parametric study was subsequently conducted for further investigation. According to the experimental and numerical results, the low ductility of HSS has a negligible effect on the tensile capacity of angles with long leg connections, whereas the tensile capacity of angles with short leg connections is reduced because of the low ductility of HSS. The test tensile capacities of the HSS welded single angles and HSS bolted single angles with long leg connections can be accurately predicted using the $1-\bar{x}/L$ rule to consider the shear lag effect. On the contrary, the predictions for HSS bolted single angles with equal and short leg connections are un-conservative. A reduction factor is proposed on the basis of the results of the tests and numerical study to consider the effect of steel grade by modifying the $1-\bar{x}/L$ rule. The modified equation provides a more accurate prediction of the test results.

ACKNOWLEDGEMENTS

I would like to express my sincere gratitude to my supervisor Dr. M. C. H. Yam for his continuous support for my M.Phil. study. Without his instruction and encouragement, the success of this research could not be accomplished. I am grateful to Prof. K. F. Chung for his patience and valuable guidance. I am also grateful to Dr. A. C. C. Lam for his technical assistance during my work in the University of Macau.

My sincere gratitude also goes to Mr. Ka Man Tou, Mr. Junhao Liu and Mr. Xuan Wang for their kind help in the University of Macau.

Thanks to Dr. Cheng Fang, Kai Wang, Qingkai Wang, Xiao Liu, Tianyu Ma, Yifei Hu for the stimulating discussions, for their constructive suggestion to my research work.

Special thanks to Qiong Sun, Keqing Zheng, Feifei Dong, Wei He, Jason Zhou, Meiling Li, Ming Luo, Yanyang Zhang, Xiao Yang and Ling Leng for their kind friendship.

Finally, I would like to express my deep gratitude to my parents, my girlfriend Yusha Zhao for their unconditional support and encouragement throughout my study.

TABLE OF CONTENTS

LIST OF FIGURES

LIST OF TABLES

CHAPTER 1 INTRODUCTION

1.1 BACKGROUND

The use of high strength steels (HSS) to construct high-rise buildings and long-span structures has been gaining popularity in the construction industry because HSS have a high strength-to-weight ratio. This property reduces the overall weight of a structure and the corresponding construction cost. Normally, HSS refer to a family of steels with a specified minimum yield stress higher than 460 MPa (EN1993-1-12, 2007). This category of steel has been available in the construction of bridges in Japan (e.g., JIS SM58 with yield stress of 600 MPa) and the United States (e.g., ASTM A514 with yield stress of 690 MPa) since the 1960s. Although these new steels were successfully applied in several bridges, their application at that time was restricted in both countries because of poor weldability (Miki et al., 2002; Galambos, et al., 1997). In the 1990s, the development of steel-making technology, such as the thermomechanical control process (TMCP) and quenching and tempering (Q&T) method, resulted in the production of steels with fine-grained microstructures. Steels with high strength, excellent toughness, improved weldability, and improved corrosion resistance can be produced by applying these advanced technologies and by adopting the appropriate combination of alloy content (Raoul and Günther, 2005). Thus far, HSS have been gradually applied in several structures, such as tall buildings, bridges, stadiums, and transmission towers, around the world (Shi and Ban, 2009). HSS have a potential to be widely used in the civil engineering industry in the future.

The major advantages of using HSS compared with normal steels (NS) as structural materials are weight reduction and savings in overall cost. Component size can be reduced by improving material strength, thereby resulting in significant reduction in the weight of a structure. According to Raoul and Günther (2005), the reduced weight can reach 20% in the case of medium- and long-span bridges. The cost of transportation and erection can be accordingly reduced with reduced weight. Further savings can be attained from the reduced amount of welding work (Raoul and Günther, 2005). In addition, HSS structures are more environmentally sustainable because of less consumption of steel/energy. This makes HSS more attractive since material/energy saving is becoming a significant issue in current building design. Moreover, structural system can be more flexible and building space can be exploited more efficiently using HSS. Many innovative and aesthetic structures can also be achieved (Galambos, et al., 1997).

The potential application of HSS covers many types of structural components, such as steel columns, hybrid steel girders, steel–concrete composite components, and steel tension members (Shi et al., 2012; Veljkovic and Johansson, 2004; Varma et al., 2002; Može and Beg, 2011). In some applications, such as beams and columns, the failure of steel structures may be governed by serviceability limit states, such as deflections or drifts. In these cases, the strength of HSS is not fully developed, and the benefits brought by high strength are reduced. Therefore, it is preferable to utilize HSS in situations in which the failing criterion is controlled by strength to take advantage of the strength of HSS efficiently. The use of HSS as tension members is considered to be a promising direction in terms of structural application. However, a significant concern that HSS possess considerably lower ductility than NS also arises. In general, a trade-off is believed to exist between ductility and strength. For example, the ultimate strain ε_u (which corresponds to the ultimate strength), the strain at fracture ε_{fr}, and the yield strength-to-ultimate strength ratio (Y/T ratio) of a typical S690 steel are approximately 8%, 15%, and 0.93, respectively, whereas those of a typical S355 steel are nearly 20%, 30%, and 0.7, respectively (Ban et al. 2011). The evident difference in ductility apparently leads to different structural performances particularly in tension members in which ductility has a significant effect on structural strength and behaviour.

Single angles are commonly used as structural tension members (e.g., truss in Figure 1.2). A critical factor that affects the tensile capacity of this type of tension member is the shear lag effect as shown in Figure 1.3. Shear lag occurs when the angles are connected by only one leg, and the unconnected part does not resist the tensile force directly but through the connected part by shear force. As a result, the stress in the unconnected part decreases from the connected heel to the extreme outstanding toe, which lags behind the stress in the connected part. Thus, the connected part can reach its ultimate strength earlier than that of the unconnected leg, and a fracture can occur in the connected part before the unconnected part develops its full capacity. The uneven stress distribution caused by the shear lag effect can obviously reduce the section capacity of angles. In addition to the shear lag effect, secondary bending caused by out-of-plane eccentricity can reduce the ultimate capacity of single angle tension members. However, normally, effect of shear lag and secondary bending are considered as one reduction factor and evaluated by a coefficient of section efficiency U which is defined as the ratio of ultimate capacity to the product of tensile strength of material and net cross-section area. A widely used equation to evaluate the shear lag effect is $1-\bar{x}/L$ rule (Eqn 1.1). This equation was proposed by Munse and Chesson (1963) and was adopted as a basis of design equations by several specifications, such as ANSI/AISC 360-10 (American Institute of Steel Constructions [AISC], 2010) and CAN/CSA-S16-14 (Canadian Standards Association [CSA], 2014). The typical definition of parameters in the equation is illustrated in Figure 1.1. The details about this equation are discussed in the chapter on the literature review.

$$U = 1 - \bar{x}/L, \tag{1.1}$$

where U is the net section efficiency, $\bar{x}$ is the out-of-plane eccentricity, and L is the length of connection.

Munse and Chesson (1963) considered connection length and out-of-plane eccentricity as the two major test parameters in their experimental programme, while influence of strength or ductility of steel was not considered. All the specimens were fabricated with NS. The shear lag effect of HSS was not examined. However, this effect may be different from that of NS because of the different ductility of the material. For single angles made of NS, good ductility allows the unconnected part to develop sufficient stress redistribution before the fracture of the connected part. Therefore, the load can be mobilized more effectively to the unconnected part. However, for single angles made of HSS, poor ductility initiates an early fracture of the connected part, thereby making load mobilization significantly less effective. The tensile capacity of single angles may decrease with decreasing ductility. In other words, the shear lag effect of single angles made of HSS may be more significant than that of single angles made of NS.

1.2 STATEMENT OF THE PROBLEM

In recent years, the demand for HSS in the construction industry has continued to grow because of the significant benefits of their usage. However, the application of HSS was developed at a relatively slow pace because of the lack of available design guidance. The latest editions of the major specifications, including ANSI/AISC 360-10 (AISC, 2010), CAN/CSA-S16-14 (CSA, 2014), AS4100-1998/Amdt 1-2012 (Standards Australia, 2012), and EN1993-1-12 in Eurocode 3 (European Committee for Standardization [CEN], 2007), cover the use of steels with yield stress of up to 690 MPa. However, the design equations of the shear lag effect are either specified to be not applicable to HSS tension members as in EN 1993-1-12 or are simply duplicated from the ones for the design of NS tension members as in the other specifications. The structural behaviours of HSS and NS tension members are expected to be different because of the different levels of ductility of material as demonstrated earlier. Thus, the design recommendations stipulated in these specifications may not be completely applicable for HSS tension members. In addition, although several studies were conducted to examine the shear lag effect of tension members, nearly all of them only focused on NS. The test data on the shear lag effect of HSS tension members found in the current studies are also inadequate. Therefore, an investigation consisting of numerical and experimental analyses is strongly required to provide a basic understanding of the shear lag effect of HSS tension members.

1.3 SCOPE AND OBJECTIVES

This thesis aims to investigate the shear lag behaviour of HSS bolted and welded single tension angles. The following are the objectives of this study:

1. To conduct a series of full-scale bolted and welded angle tension member tests with steel grade, connection length, and out-of-plane eccentricity as the test parameters;
2. To develop an accurate finite element model to predict the behaviour of the HSS and NS bolted and welded single angle specimens and to conduct a parametric study.
3. To compare the test results of specimens made of HSS with the $1 - \bar{x}/L$ rule to examine its applicability; if necessary, a new or modified equation may be proposed to assess the shear lag effect.

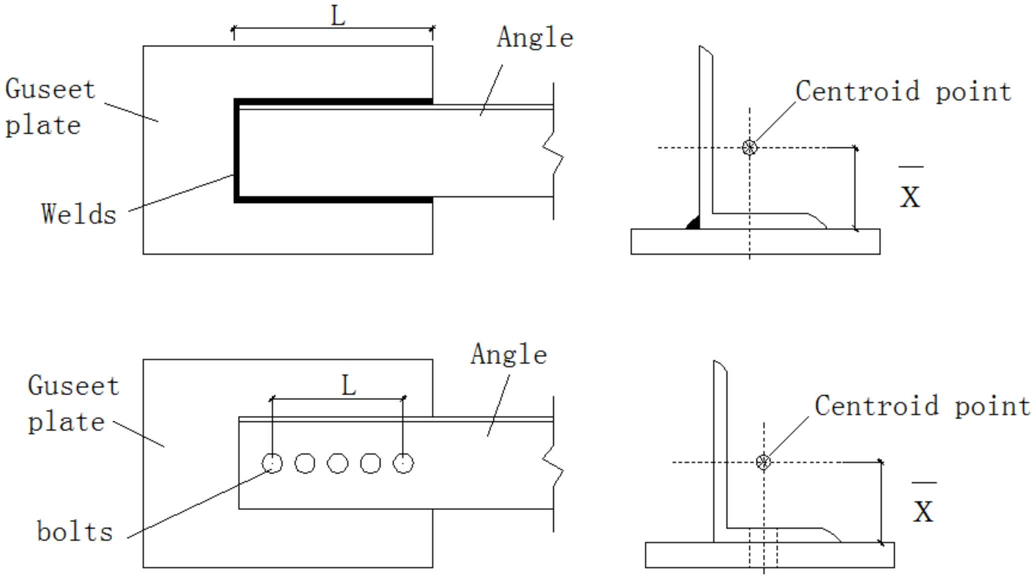

Figure 1.1 Typical definitions of parameters of bolted and welded angles

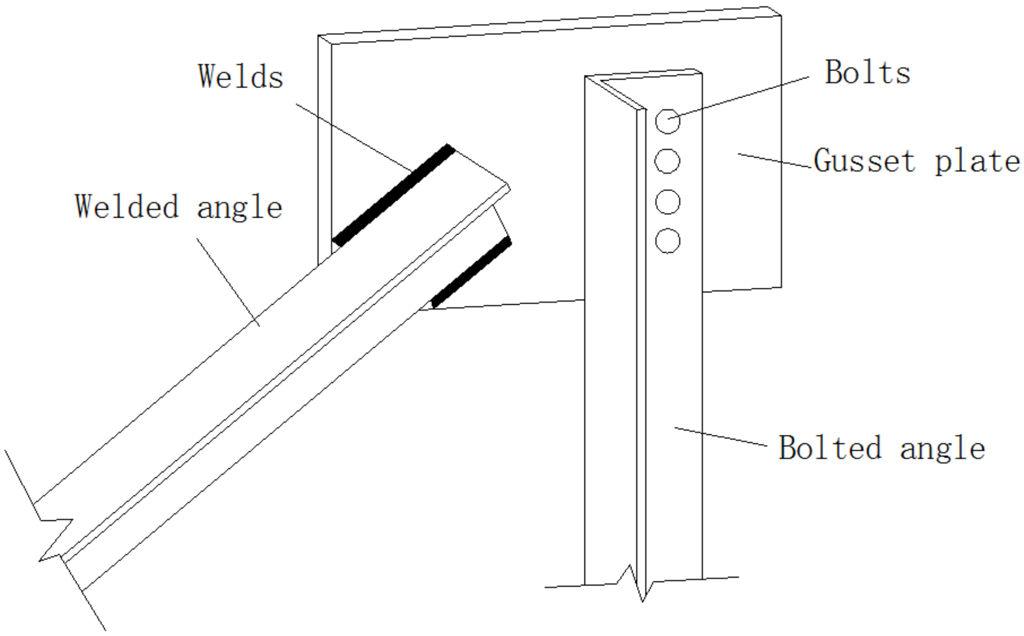

Figure 1.2 Single angles used in typical truss joint

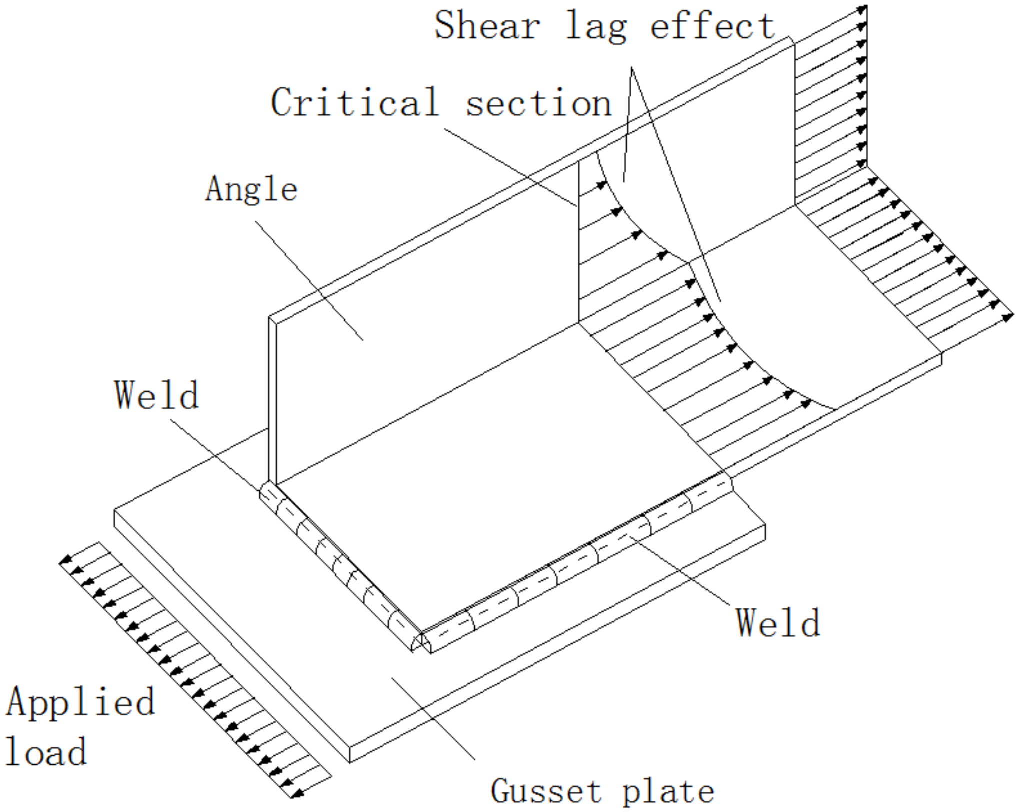

Figure 1.3 Stress distributions in welded single angle due to shear lag effect

CHAPTER 2 LITERATURE REVIEW

2.1 INTRODUCTION

Three areas are reviewed in this chapter: HSS material property, HSS tension members, and shear lag of tension members with bolted and welded connections. For the HSS material property, particular attention is given to ductility, which is the major concern of using HSS for tension members. Subsequently, the tensile behaviours of HSS connections are summarized given that the structural behaviours of connections made of HSS and NS may be different because of different ductility. Other structural behaviours of HSS members, such as buckling behaviour or seismic behaviour, are not included in this study. Finally, a comprehensive review of the shear lag effect of bolted and welded tension members is presented. The literature on the shear lag effect of HSS connections is scarce, and thus this review mainly focuses on NS connections.

2.2 MATERIAL

The earliest application of HSS to construction dates back to the 1960s in Japan and the United States (Miki et al. 2002; Shi et al. 2014). HSS are used on bridge constructions to reduce the size of bridge girders, thereby resulting in significant weight reduction. Since then, many studies have been conducted to optimize HSS property. The strength, toughness, weldability, and corrosion resistance of HSS have been continuously improved. At present, the available HSS grade in the United States includes Grade 70W, HPS 70W, 100W, and HPS100W (ASTM A709/709M; ASTM A514/514M). In Europe, the available HSS grade includes S460, S500, S550, S620, S690, S890, and S960. Eurocode 3 (CEN, 2007) only covers the use of steel types up to S690. In both the United States and European specifications, HSS can be manufactured through TMCP or Q&T processes. Both metallurgical techniques aim to create extremely fine-grained microstructures, which can improve steel strength without adding more alloy content (particularly carbon content). In general, increased alloy content can provide high strength but poor performance, particularly in weldability and toughness. Compared with the steels produced through conventional processes (e.g., normalizing), the steels produced by refining grain size and by reducing alloy content can obtain the same strength but with enhanced toughness and weldability (Willms, 2009). Nevertheless, a trade-off always exists between the strength and ductility of steel materials.

In general, the common indexes to evaluate steel ductility include ultimate strain ε_u, which corresponds to the ultimate strength, and the strain at fracture ε_{fr}. The stress–strain relationships of different types of HSS were examined by several researchers (Sooi et al., 1995; Fukumoto, 1996; Langenberg et al., 2000; Sause and Fahnestock 2001; Sedlacek and Muller, 2001; Ban et al. 2011). Figure 2.1 shows a representative comparison of the stress–strain curves of typical HSS (i.e., HSLA80, HT780, S690, and S960) and typical NS (i.e., A36) (Sooi et al., 1995; Fukumoto, 1996; Chen, 1997; Ban et al. 2011). Figure 2.1 illustrates that both ultimate strain ε_u and strain at fracture ε_{fr} decrease evidently with the increased steel strength at approximately 7% and 15%, respectively, for HSS steels and approximately 20% and 30%, respectively, for NS steels.

Other important indexes include Y/T ratio and the reduction of area (Z). Y/T ratio is commonly used as a test parameter in experiments to represent the tensile property of steels (Brockenbrough, 1995). According to Dexter et al. (2002), Y/T ratio is related to ultimate strain. HSS are considered to possess a high Y/T ratio and a low ultimate strain. For instance, the average Y/T ratio of A514 steel with yield stress of 690 MPa is approximately 0.94, and that of HPS70W steel with yield stress of 485 MPa is nearly 0.84. Moreover, the average Y/T ratio of an NS with yield stress of 345 MPa is approximately 0.77 (Dexter et al., 2002). Similarly, Ban et al. (2011) summarized from several existing test results the Y/T ratios of different types of steels with yield strength ranging from 420 MPa to 960 MPa. The results showed that the average Y/T ratios of coupons with yield stress of 420, 460, 690, and 960 MPa are approximately 0.73, 0.80, 0.93, and 0.93, respectively. For the reduction of area, Langenberg (2001) determined that the values also slightly decrease with the increased steel strength at 75%, 70%, and 65% for S355, S690, and S960, respectively.

In conclusion, a comprehensive comparison of indexes of ductility indicates that the ductility of HSS is considerably lower than that of NS. Therefore, a concern arises on the effect of low ductility of HSS materials on the structural behaviour of HSS tension members, including the shear lag effect. The following sections present a comprehensive review of the literature on HSS tension members and the shear lag effect of tension members.

2.3 HSS TENSION MEMBERS

Kouhi and Kortesmaa (1990) conducted a series of tests on double-shear bolted connections. Steel with yield stress of 640 MPa was used. The bolts were arranged in two configurations: two in one line and four in two lines. The bearing resistance and block shear resistance of the specimens were evaluated. The test results were compared with the predictions evaluated on the basis of several major specifications at that time, including Eurocode 3 (Commission of the European Communities, 1989) and AISC-LRFD (AISC, 1986). Eurocode 3 presented a safe estimation on the bearing resistance of the specimens. Both Eurocode 3 and AISC-LRFD provided conservative results for the block shear resistance of the specimens. However, the estimation of Eurocode 3 was apparently conservative for design purposes, whereas that of AISC-LRFD was satisfactory.

Kim and Yura (1999) investigated the bearing strength of one-bolt and two-bolt lap plate connections with various end distances and bolt spacings. Nine specimens were fabricated using HSS with yield stress of 483 MPa and ultimate stress of 545 MPa. Two types of bearing strengths were presented: bearing strength at ultimate load and bearing strength at 6.35 mm-hole deformation. The test results showed that bearing strength at 6.35 mm hole-displacement was not affected by steel strength. In addition, the deformation capacities of specimens made of different types of steel were nearly the same. The test results were also compared with the predicted results by Eurocode3 (CEN, 1992) and AISC-LRFD (AISC, 1993), and the predictions of both specifications were conservative.

Aalberg and Larsen (2001, 2002) also studied the tensile behaviour of HSS lap joint connection with one or two bolts. Weldox700 (with yield stress of 700 MPa) and Weldox1100 (with yield stress of 1100 MPa) were used. The authors determined that the elongation at ultimate load of the specimens decreases considerably with increased steel grade. The reduction could reach 39% and 43% for Weldox700 and Weldox1100, respectively, compared with that of S355 steel. Nevertheless, the elongation at fracture was not largely affected by steel strength. Additionally, the predictions of AISC-LRFD (A1SC, 1993) and Eurocode 3 (CEN, 1992) were accurate in those specimens.

Puthli and Fleisher (2001) evaluated the bearing strength of bolted plates fabricated with S460 steel. In total, 25 specimens were tested. All the plates were connected by two 10.9 bolts in the transverse direction with various bolt spacings. The test results indicated that the minimum end distance and bolt spacing regulated in the Eurocode3 (CEN, 1992) were also applicable to bolted plates made of S460. No reduction of bearing strength was detected when $e_2 \geq 1.2d_0$ or $p_2 \geq 2.4d_0$ (where e_2 is the edge distance, p_2 is the bolt spacing, and d_0 is the bolt hole diameter). The reduction of bearing strength when $e_2 \leq 1.5d_0$ or $p_2 \leq 3.0d_0$ specified in Eurocode 3 should be decreased.

Moreover, the limitations for reduction recommended by the authors were $e_2 = 1.0d_0$ and $p_2 = 2.0d_0$.

Dexter et al. (2002) investigated the ductility of HSS tension members. A total of 14 wide plates were tested. These plates were fabricated with steels using HPS70W, HPS100W, and Grade 50 with yield stress of 485, 690, and 345 MPa, respectively. The main parameters were Y/T ratio and A_n/A_g (ratio of net section area to gross section area). These parameters were varied by drilling different numbers of holes in the plates. The ductility of wide plates fabricated with HPS70W could meet the minimum requirements of AISC specification (AISC, 1998). The specification presented a conservative prediction of the tensile capacity of HPS70W wide plates. The test results also indicated that the ductility of the specimens could be represented well by the ratio of $\mathrm{A_n/A_g}$ to Y/T ($(\mathrm{A_n/A_g})$/(Y/T)). Sufficient ductility could be achieved when the $(\mathrm{A_n/A_g})$/(Y/T) ratio is 1 or above.

Može, Beg, and Lopatič (2007) tested 20 tension splices with one or two bolts in double shear to investigate the ductility and the net cross-section strength of HSS lap connections. The actual yield stress and ultimate stress of steel were 847 and 885 MPa, respectively. The bolts were arranged in the loading direction. Local ductility was not significantly influenced by low f_u/f_y ratio. Moreover, all the failures were ductile and were similar to those of specimens made of NS. A statistical analysis was conducted to validate the net cross-section design equation $\left(N_{t,Rd} = 0.9A_{net}f_u/\gamma_M\right)$ adopted in prEN1993-1-12 (CEN, 2006). The design equation was conservative with a partial factor γ_{M2} of 1.25.

Može and Beg (2010) examined the applicability of the bearing resistance equation stipulated in EN 1993-1-8 (CEN, 2005) to HSS connections made of S690 steel. A total of 38 bolted connections with one or two bolts were tested.

Various geometric parameters, including end distance, edge distance, and bolt spacing, were examined. Net section failure and bolt hole bearing failure were the main failure modes observed in the experiments. The predicted bearing strengths by EN 1993-1-8 were conservative for the design. Subsequently, a new equation, which is a function of the ratio of end distance to edge distance, was proposed by the authors to predict the bearing strength of HSS bolted connections based on the test results. Then, Može and Beg (2011) investigated the behaviour of bolted connections made of S690 steel with three or four bolts. A total of 26 specimens were tested. A finite element model was also established to verify the stress distribution around the bolts. The local ductility was sufficient to achieve stress redistribution among all the bolt holes. The modified equation (Može and Beg, 2010), which was derived from HSS bolted connections with one or two bolts, was also applicable to HSS bolted connections with three or four bolts but with additional coefficients.

Yan and Young (2011) carried out an experiment to investigate the structural behaviours of thin sheet steels under elevated temperatures. A total of 120 single shear bolted connections and 30 coupons were tested under elevated temperatures ranging from 22 to 900℃. The proof stress and tensile stress obtained from coupon specimens with three different thicknesses at normal temperature ranged from 504 to 718MPa and from 543 to 718MPa, respectively. The test results were compared with the predictions by American, Australian and European specifications and general conservative results were found. In addition, Yan and Young (2012) also conducted a numerical study based on the previous test results. A parametric study which consisted of 182 bolted connections under 7 different temperatures were performed to study the bearing strength of thin sheet steel bolted connections. Bearing factors respecting the influence of elevated temperatures were proposed. The proposed equations provided more accurate predictions than the current specifications.

Cai and Young (2013, 2014) studied the structural behaviours of stainless steel bolted connections under both ambient and elevated temperatures. A series of single shear and double shear bolted connections with various bolt arrangement were included in the experiment. Three types of stainless steels with proof stress all over 460MPa were used. It was observed that the predicted strengths from current specifications were generally conservative at both ambient and elevated temperatures.

2.4 SHEAR LAG EFFECT OF A BOLTED CONNECTION

Nelson (1953) tested 18 single angle tension members with a bolted connection to investigate the strain distribution and deformation of specimens at all stages up to failure. The author noted that compressive yield stress was reached in the unconnected leg for some specimens. An empirical equation, which is a function of the ratio of unconnected area to connected area and the number of bolts, was proposed based on test results. The equation is as follows:

$$\mathrm{R} = 1/(1 + \mathrm{r}/\mathrm{n}) \,, \tag{2.1}$$

where R is the net section efficiency, r is the ratio of outstanding area to connected area, and n is the number of bolts in line.

The most widely used equation that considers the shear lag effect was proposed by Chesson and Munse (1963), and this equation was adopted by ANSI/AISC 360-10 (AISC, 2010) and CAN/CSA-S16-14 (CSA, 2014). Based on 218 tests of rivet and bolted end connection angles, the out-of-plane eccentricity $\bar{\mathrm{x}}$ and connection length L were considered to affect the shear lag effect most significantly and were selected for the development of the net section efficiency equation as mentioned earlier:

$$\mathrm{U} = 1 - \bar{\mathrm{x}}/\mathrm{L}, \tag{2.2}$$

where U is the net section efficiency, $\bar{x}$ is the out-of-plane eccentricity, and L is the connection length.

Out-of-plane eccentricity is the perpendicular distance from the face of the connected part to the centroid point of the section, and connection length is the distance between the two outmost bolts as shown in Figure 1.3. This equation was then validated using more than 1,000 test data. Good accuracy with deviation under 10% was achieved. In the AISC specification, the coefficient U could be taken as the larger value between the value obtained from this equation and 0.6 for connections with three fasteners; 0.8 for connections with four or more fasteners.

Madugula and Mohan (1988) discussed the test results from the experiments conducted by Nelson (1953), Mueller and Wagner (1985), and Hanson (1987). In total, 61 test results of single-angle connections were summarized. By comparing these results with various specifications, including AISC-LRFD (AISC, 1984), CAN3-S16.1-M84 (CSA, 1984), and BS5950 (British Standard Institution [BSI], 1985), the authors determined that different equations should be developed for unequal leg angles to distinguish different cases, that is, being connected by a short or a long leg. Block shear failure could also occur for certain arrangements of bolts.

Kulak and Wu (1997) tested 24 single and double angle tension members. The effects of several parameters, including out-of-plane constraint, angle thickness, angle disposition, and connection length, were verified. Out-of-plane constraint and angle thickness had a slight effect on section efficiency, and the effect of angle disposition and connection length was significant. In addition, stress distribution was examined in different cases through finite element analysis. The authors determined from the test results that uniform yield stress was developed in the whole outstanding area in the critical section when four or more bolts were connected, and that half of the yield stress could be used for the same area when a few bolts were connected. On the basis of this observation, they proposed a new equation as follows:

$$P_u = F_u A_{cn} + \beta F_y A_o, \tag{2.3}$$

where P_u is the predicted ultimate load of the member, F_u is the ultimate tensile strength, F_y is the yield strength, A_o is the net area of the outstanding leg, and β = 1 for members with four or more bolts per line or β = 0.5 for members with two or three bolts per line.

Orbison, Barth, and Bartels (2002) investigated the effect of in-plane eccentricity, which is often neglected in the current shear lag equations. A total of 22 bolted connections with a WT section (tee section cut from wide flange beam) with various connection lengths and in-plane eccentricity were tested. The in-plane eccentricity strongly affected the net section rupture strength when it exceeded 45 mm. The AISC specification at that time lacked consideration of this reduction. Thus, the authors proposed the following shear lag effect equations by considering in-plane eccentricity.

For punched specimens,

$$U = 0.48 - 0.19\bar{x} + 0.049L \leq 0.9 \tag{2.4}$$

For drilled specimens,

$$U = 0.50 - 0.19\bar{x} + 0.054L \leq 0.95 \tag{2.5}$$

In these equations, U is the net section efficiency, $\bar{x}$ is the in-plane eccentricity, and L is the connection length

2.5 SHEAR LAG EFFECT OF A WELDED CONNECTION

Davis and Boomsliter (1934) investigated the ultimate strength of welded and riveted angle tension members. Various angle arrangements, including single, double, and four angles with one or two connecting plates, were designed. 6 riveted and 7 welded connections were tested, but 4 welded angle specimens failed in the welds. The results indicated that the efficiencies of single angles and double angles with two angles on the same side, both welded and riveted, were between two-thirds and three-quarters.

Gibson and Wake (1942) investigated welded angles with various weld arrangements to study the effect of balanced and unbalanced weld arrangements. 15 single and 9 double angles were tested and designed to fail in the welds. The results showed that the efficiency of balanced connections was nearly the same as that of the unbalanced connections. In addition, out-of-plane eccentricity had a major effect on the tensile capacity of welded angles.

Regan and Salter (1984) tested 17 welded single angle tension members with welds on three sides. Various sizes of angles ranging from 25 mm × 25 mm × 8 mm to 125 mm × 75 mm × 8 mm were investigated to examine the effect of the ratio of connected leg length to outstanding leg length. The test results showed that the reduction of section efficiency of the welded angle specimens did not exceed 10%. The test results were compared with the design provisions stipulated in BS449 (BSI, 1969). In the specification, the test efficiency was evaluated by calculating the effective area a_e. This method considers that stress is uniformly distributed within the effective area of the section instead of unevenly distributed within the full area of the section. Therefore, tensile capacity is calculated as follows:

$$P_t = p_y \mathrm{a_e}, \tag{2.6}$$

where $\mathrm{P_t}$ is the tensile capacity, $\mathrm{p_y}$ is the yield strength, and a_e is the effective area.

Based on the test results, a new equation was proposed to calculate the effective area:

$$a_e = a_1 + 0.8a_2, \tag{2.7}$$

where a_1 is the area of the connected leg, and a_2 is the area of the outstanding leg.

Easterling and Gonzalez (1993) tested 27 small-sized welded tension members, including plates, angles, and channels. Different weld arrangements (i.e., longitudinal, transverse, and combination of longitudinal and transverse) were used for different types of tension members. For angles, all except one used the balance weld arrangement. The test results of the angle specimens were well predicted by the AISC provisions at that time. In addition, efficiency was only slightly affected by weld length when it exceeded plate width; by contrast, efficiency was not affected by the transverse weld when both transverse and longitudinal welds existed. For specimens with only transverse welds, failure was not controlled by shear lag. Instead, the shear strength of the weld controlled the ultimate strength of the specimens. Moreover, an upper limit of 0.9 for the shear lag coefficient was proposed.

Zhu et al. (2009) investigated welded single angle tension members. 13 specimens were tested with various parameters, including long or short leg connection, balanced or unbalanced arrangement, and longitudinal weld length. The test results indicated that efficiency could be improved with increased connection length when a short leg was connected, but it was not affected when a long leg was connected. Moreover, when members were connected by a long leg, efficiency would be higher than when members were connected by a short leg. Moreover, a balanced arrangement could improve the tensile capacity of members connected with a short leg and could increase the ductility of the angle specimens.

Fang et al. (2013) conducted an experiment using 12 single angle and 8 single tee tension members with welded connections. All angles were connected by a short leg. The parameters included weld arrangement and steel strength. Among the specimens, two were fabricated using HSS with yield stress of 484 MPa and ultimate stress of 693 MPa. The test results indicated that the efficiency and elongation of HSS members were obviously lower than those of NS members. The results also showed that, compared with unbalanced welded tension members, balanced ones could improve efficiency by 2%–12% at an average of 5.9%. Beneficial effects were found when the transverse weld was replaced by a longitudinal weld on the condition that the weld capacity remained unchanged.

2.7 SUMMARY

This chapter presented the typical material property of HSS. The ductility of HSS was mainly examined through four major indexes: ultimate strain, strain at fracture, Y/T ratio, and reduction of area. All existing data showed that the ductility of HSS was significantly lower than that of NS. Furthermore, a comprehensive review of the structural behaviour of tension members made of HSS was conducted. Experiments on tension plates with bolted connections were conducted to investigate the net section strength, bolt hole bearing strength, and block shear strength of HSS plates. The applicability of major specifications was also evaluated. The results indicated that the estimations made by current specifications on the tensile capacity of HSS plates were conservative. However, existing studies did not cover tension angles.

An extensive review of the shear lag effect of NS tension members was also presented. Bolted and welded single angles were tested with various parameters including connection length and out-of-plane eccentricity. Several equations and suggestions were proposed, and some of them were adopted in major specifications. However, all these studies only focused on the behaviour of angles made of NS, and the equations of all the specifications, including the $1-\bar{x}/L$ rule, were based on the test results of the specimens made of NS. Therefore, increased attention should be given on the shear lag effect of HSS angles. Additional test data are required to form a better understanding of the structural behaviour of HSS angles and to evaluate the applicability of current specifications to HSS angles.

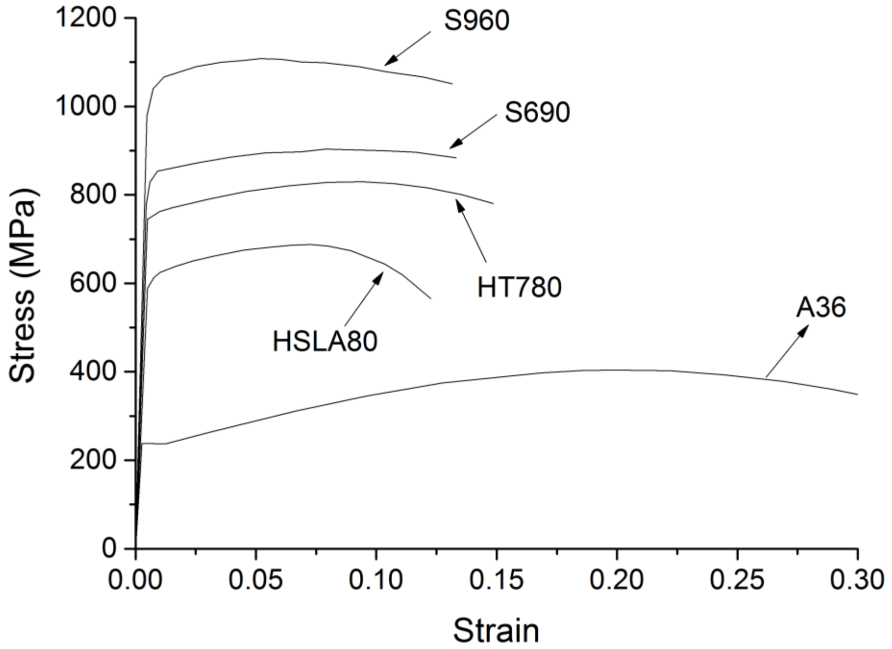

Figure 2.1 Stress-strain curves of several types of HSS (Sooi et al., 1995; Fukumoto, 1996; Chen, 1997; Ban et al. 2011)

CHAPTER 3 EXPERIMENTAL PROGRAMME

3.1 SPECIMEN DESIGN

The main purpose of this experimental programme is to investigate the shear lag effect of bolted and welded single angles made of HSS. A total of 9 bolted single angles and 9 welded single angles were tested. For each connection type, 7 specimens were made of S690 steel, and the remaining two specimens were made of S275 steel. Typical configurations of the bolted and welded angle specimens are shown in Figures 3.1 and 3.2, respectively.

As mentioned previously, the test parameters included steel grade, connection length, and out-of-plane eccentricity. These parameters were chosen on the basis of the information obtained from the literature review. In comparing the structural behaviours between the specimens made of HSS and those made of NS, two comparison groups were designed with the same configuration and different steel grades (S275 and S690) for each type of connection (bolted and welded). The test results acquired by this test programme would allow the review of the applicability of the $1-\bar{x}/L$ rule to estimating the tensile capacity of the bolted and welded HSS angles. Different specimen section sizes and dispositions (i.e., long or short connections) were employed to vary the out-of-plane eccentricity. The section sizes of specimens are shown in Table 3.1. Different bolt spacing and weld lengths were used to examine the effect of connection length on the strength and behaviour of the bolted connection specimens and the welded connection specimens, respectively. The details of the test parameters of the bolted and welded angle specimens are presented in Tables 3.2 and 3.3, respectively.

Two types of section sizes were chosen for the test programme, namely, 80 mm x 60 mm x 8 mm and 100 mm x 65 mm x 8 mm. All the angles were unequal angles with a long leg or a short leg connection. The number of bolts was five for all the bolted connection specimens. Three bolt spacings of 60, 75, and 90 mm were used with the corresponding connection lengths of 240, 300, and 360 mm, respectively. For the welded connection specimens, the unbalanced weld arrangement with one transverse weld and two longitudinal welds of identical weld length was used because the unbalanced weld arrangement is used more often in real construction than the balanced one. The in-plane eccentricity induced by the unbalanced weld arrangement is believed to be relatively small and hence not considered. The weld lengths of 220, 300, and 380 mm were examined in the test programme. In ensuring net section failure, other unexpected failure modes were eliminated through the proper detailed design of the test specimens. The length of all specimens was designed to match the test setup and to ensure that sufficient distance was provided between the two ends of the specimen. The clear length of the specimen between the two gusset plates was 800 mm. All the gusset plates were made of S355 steel, and they were all set to be 400 mm wide and 16 mm thick to ensure that the gusset plate was loaded within the elastic range of the material.

The bolted and welded angle specimen designations and details are listed in Tables 3.2 and 3.3, respectively. The typical geometric configurations of the bolted and welded tension members are illustrated in Figures 3.1 and 3.2, respectively. The letters “A, B, C, and D” for designation represent different connection types (bolted or welded) combined with different steel strengths (S690 or S275). “A” and “B” represent bolted angles made of HSS and NS, respectively. “C” and “D” represent welded angles made of HSS and NS, respectively. The first numbers “1” and “2” represent sections 80 mm x 60 mm x 8 mm and 100 mm x 65 mm x 8 mm, respectively. The bolt spacing of the bolted angles or the connection length of the welded angles is represented by the second number. The final letters “S” and “L” stand for short leg connection and long leg connection, respectively. For example, in specimen A1-60L, the angle was fabricated with S690 steel, and the section size was 80 mm x 60 mm x 8 mm.

The specimen was long leg connected by bolts with a bolt spacing of 60 mm.

Tension coupon tests were conducted according to ASTM A370 (American Society for Testing and Materials [ASTM], 2015). The coupons of steel S690 were extracted from 8mm thick steel plates along the longitudinal direction whereas the coupons of steel S275 were cut from the untested hot-rolled angles. The Young’s modulus, yield strength, ultimate strength and ultimate strain were measured.

3.2 TEST SETUP AND INSTRUMENTATION

A SATEC universal testing machine with a tensile capacity of 2000 kN was employed for the tension tests as shown in Figure 3.3. Two end fixtures were connected by seven Grade 8.8 M24 bolts to the gusset plates, where the specimens were connected by either bolts or weld.

The applied load was recorded by the built-in load cell of the testing machine. The elongation of the specimen was measured by the inner transducers of the machine, which recorded the total extension between the two crossheads of the machine. The typical layouts of strain gages on the bolted and welded angle specimens are illustrated in Figures 3.4 and 3.5, respectively. For the welded members, six gages were mounted, with three gages on the connected leg and three gages on the outstanding leg, in the critical section and the mid-length section. For the bolted members, only two gages were mounted on the connected leg and three gages were mounted on the unconnected leg because of the presence of bolt holes at the critical section. The strain layout in the mid-length section was the same as that of the welded members.

3.3 TEST PROCEDURE

The test procedures for each specimen were similar. A specimen was installed in the test machine and aligned with the vertical loading direction. Preload of approximately 100 kN was applied to make each bolt in the bearing and to eliminate major slips between bolts and bolt holes. Subsequently, the preload was released to zero, and all the readings were reset to zero. The loading process consisted of two stages: load control before yielding and stroke control after yielding. During the first stage, the load increment of the specimens with different ultimate capacities was varied to ensure at least five loading steps within the stage. When the yielding of the specimens started, the loading speed was set to 1 mm per min, and each loading step lasted for 1 min or 2 min for HSS or NS specimens, respectively. After each loading step, the stroke was held constant at regular intervals to record the static load. The test was stopped when a large-scale fracture occurred in any section of the specimens.

Table 3.1 Section sizes of specimens

Specimen	Connected leg (mm)	Unconnected leg (mm)	Thickness (mm)	Note
A1-60L	80.00 80.73	60.00 60.73	8.00 8.09	Nominal Measured
A1-75L	80.00 79.48	60.00 60.30	8.00 8.04	Nominal Measured
A1-90L	80.00 80.57	60.00 59.93	8.00 8.05	Nominal Measured
A1-75S	60.00 60.30	80.00 79.48	8.00 7.99	Nominal Measured
A2-60S	65.00 63.00	100.00 99.00	8.00 8.08	Nominal Measured
A2-75S	65.00 65.00	100.00 99.00	8.00 7.96	Nominal Measured
A2-90S	65.00 64.00	100.00 99.00	8.00 8.10	Nominal Measured
B1-75L	80.00 78.00	60.00 60.00	8.00 5.98	Nominal Measured
B2-75S	65.00 65.00	100.00 101.00	8.00 5.60	Nominal Measured
C1-220L	80.00 80.00	60.00 60.00	8.00 8.10	Nominal Measured
C1-300L	80.00 80.00	60.00 60.00	8.00 8.05	Nominal Measured
C1-380L	80.00 80.00	60.00 60.00	8.00 8.015	Nominal Measured
C1-300S	60.00 60.00	80.00 80.00	8.00 8.056	Nominal Measured
C2-220S	65.00 64.62	100.00 101.20	8.00 8.06	Nominal Measured
C2-300S	65.00 65.00	100.00 100.00	8.00 8.00	Nominal Measured
C2-380S	65.00 65.00	100.00 100.00	8.00 8.02	Nominal Measured
D1-300L	80.00 78.77	60.00 60.84	8.00 7.98	Nominal Measured
D2-300S	65.00 65.82	100.00 101.16	8.00 7.68	Nominal Measured

Table 3.2 Arrangement of bolted angle specimens

Specimen	Angle size (mm)	Steel grade	Angle length (mm)	Connected leg length (mm)	Number of bolts	Spacing (mm)	Connection Length (mm)
A1-60L	80*60*8	S690	1520	80	5	60	240
A1-75L	80*60*8	S690	1640	80	5	75	300
A1-90L	80*60*8	S690	1760	80	5	90	360
A1-75S	80*60*8	S690	1640	60	5	75	300
A2-60S	100*65*8	S690	1520	65	5	60	240
A2-75S	100*65*8	S690	1640	65	5	75	300
A2-90S	100*65*8	S690	1760	65	5	90	360
B1-75L	80*60*8	S275	1640	80	5	75	300
B2-75S	100*65*8	S275	1640	65	5	75	300

Table 3.3 Arrangement of welded angle specimens

Specimen	Angle size (mm)	Angle length (mm)	Steel grade	Connected leg length (mm)	Connection Length (mm)
C1-220L	80*60*8	1520	S690	80	220
C1-300L	80*60*8	1640	S690	80	300
C1-380L	80*60*8	1760	S690	80	380
C1-300S	80*60*8	1640	S690	60	300
C2-220S	100*65*8	1520	S690	65	220
C2-300S	100*65*8	1640	S690	65	300
C2-380S	100*65*8	1760	S690	65	380
D1-300L	80*60*8	1640	S275	80	300
D2-300S	80*60*8	1640	S275	65	300

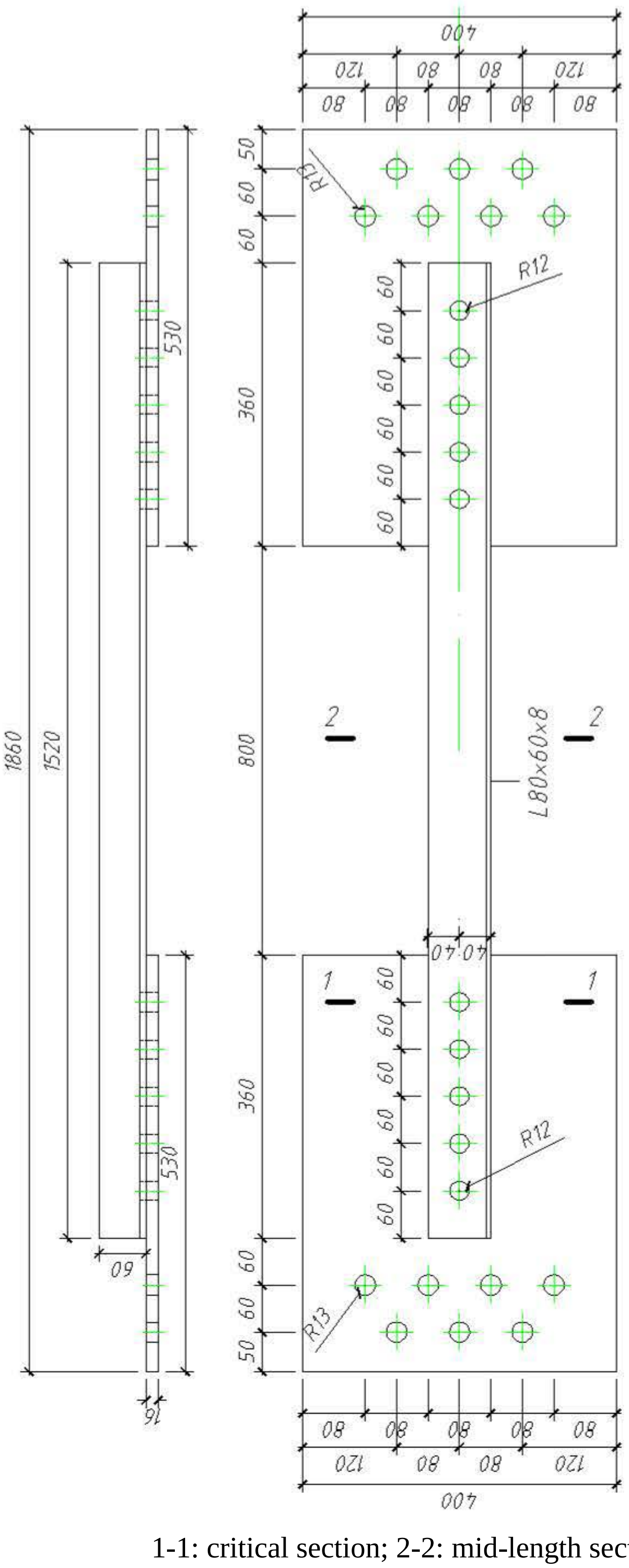

1-1: critical section; 2-2: mid-length section

Figure 3.1 Typical configuration of the bolted angle specimens

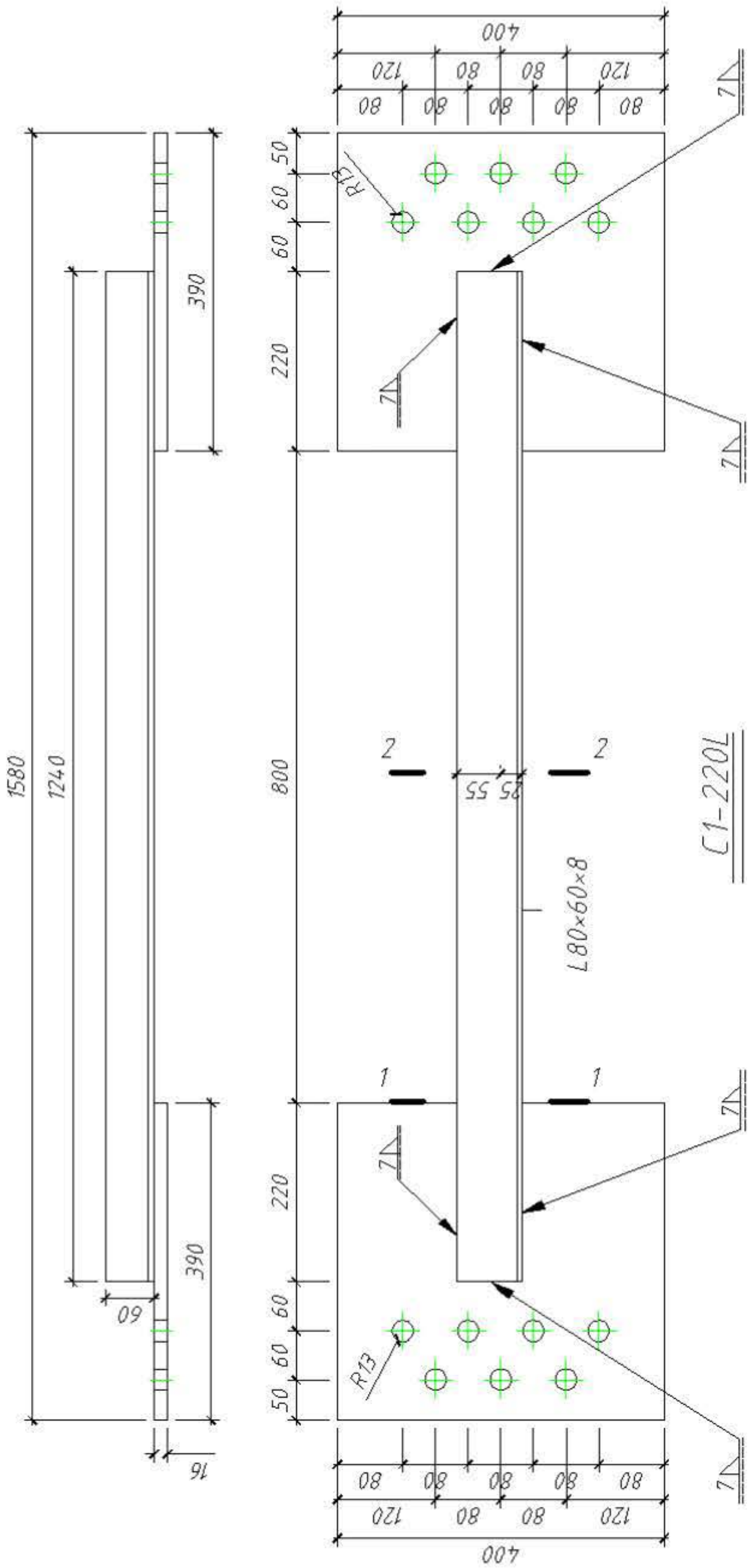

1-1: critical section; 2-2: mid-length section

Figure 3.2 Typical configuration of the welded angle specimens

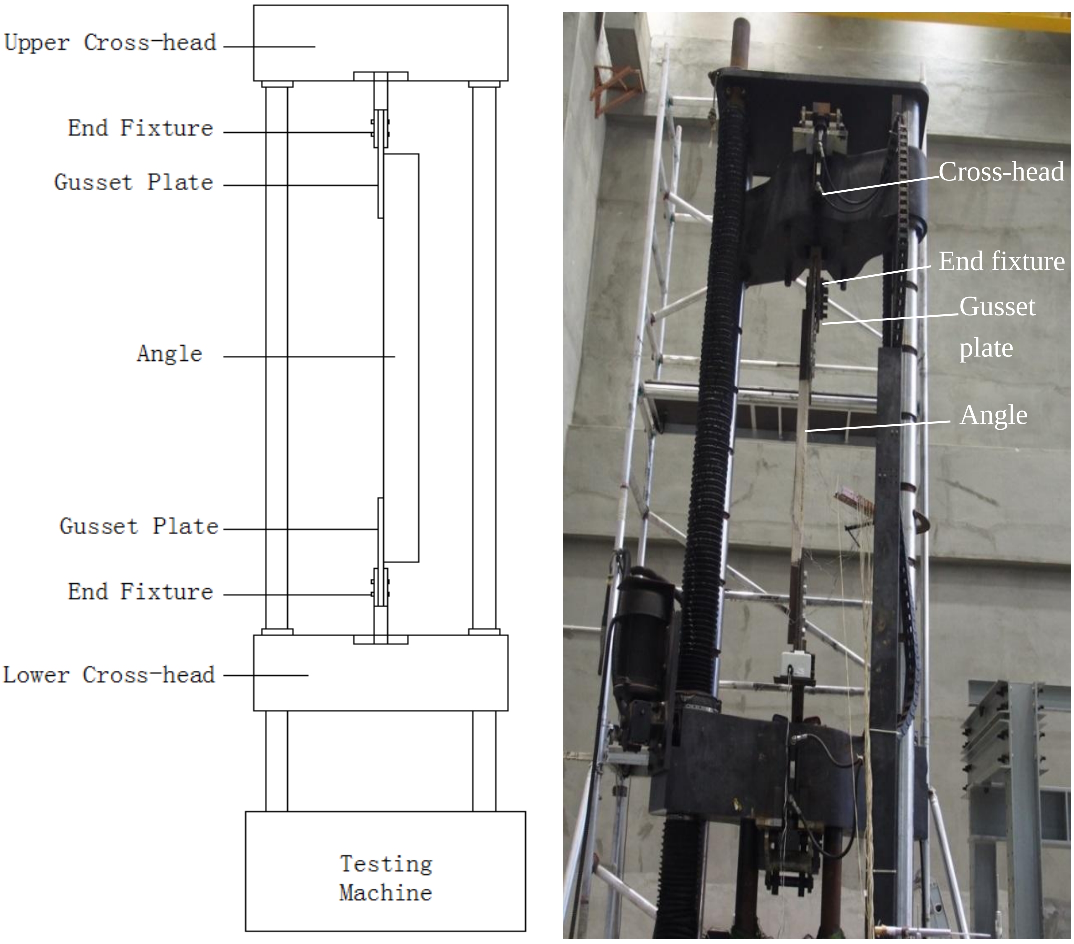

Figure 3.3 Schematic and photo of test setup

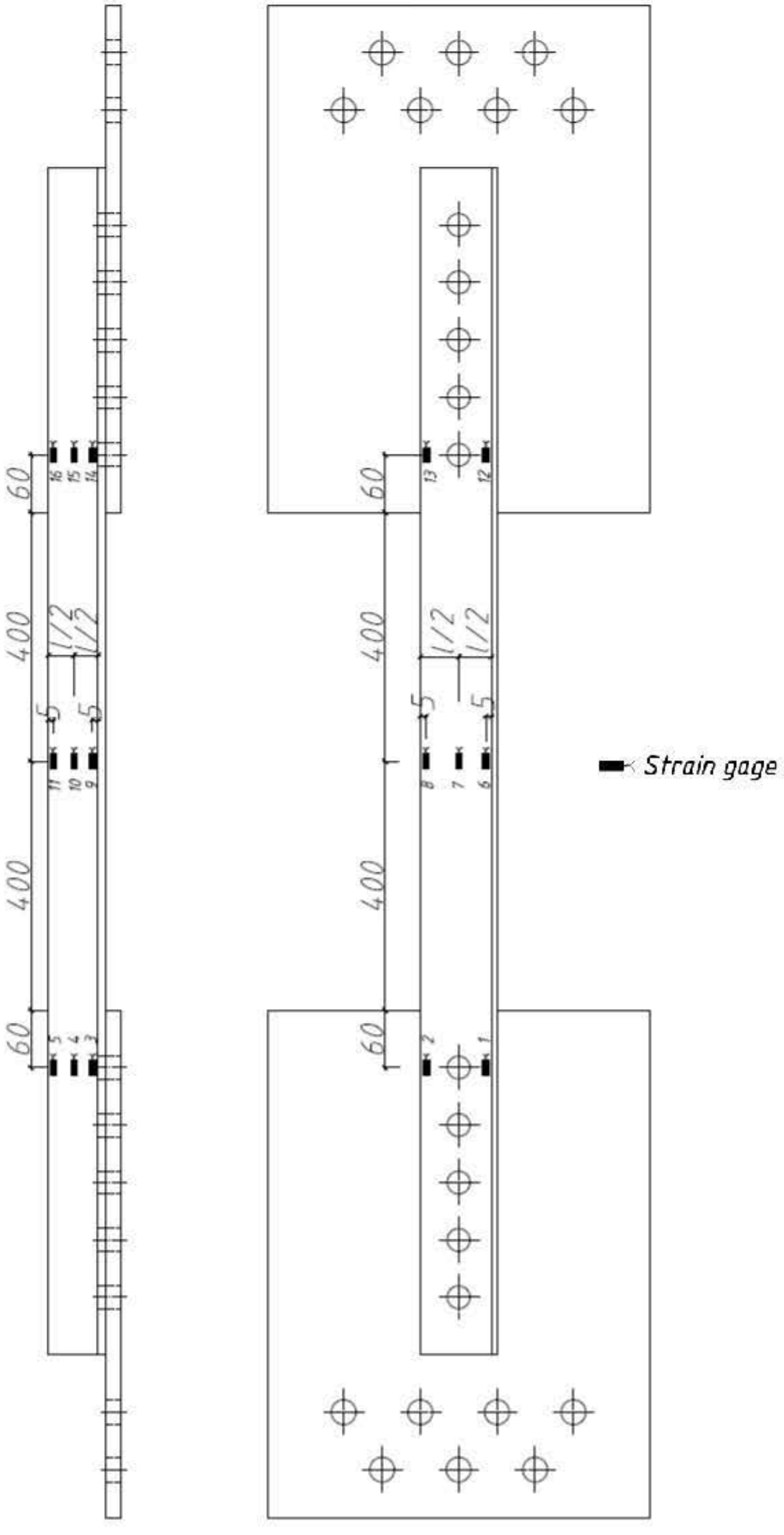

Figure 3.4 Layout of stain gages on the bolted angle specimens

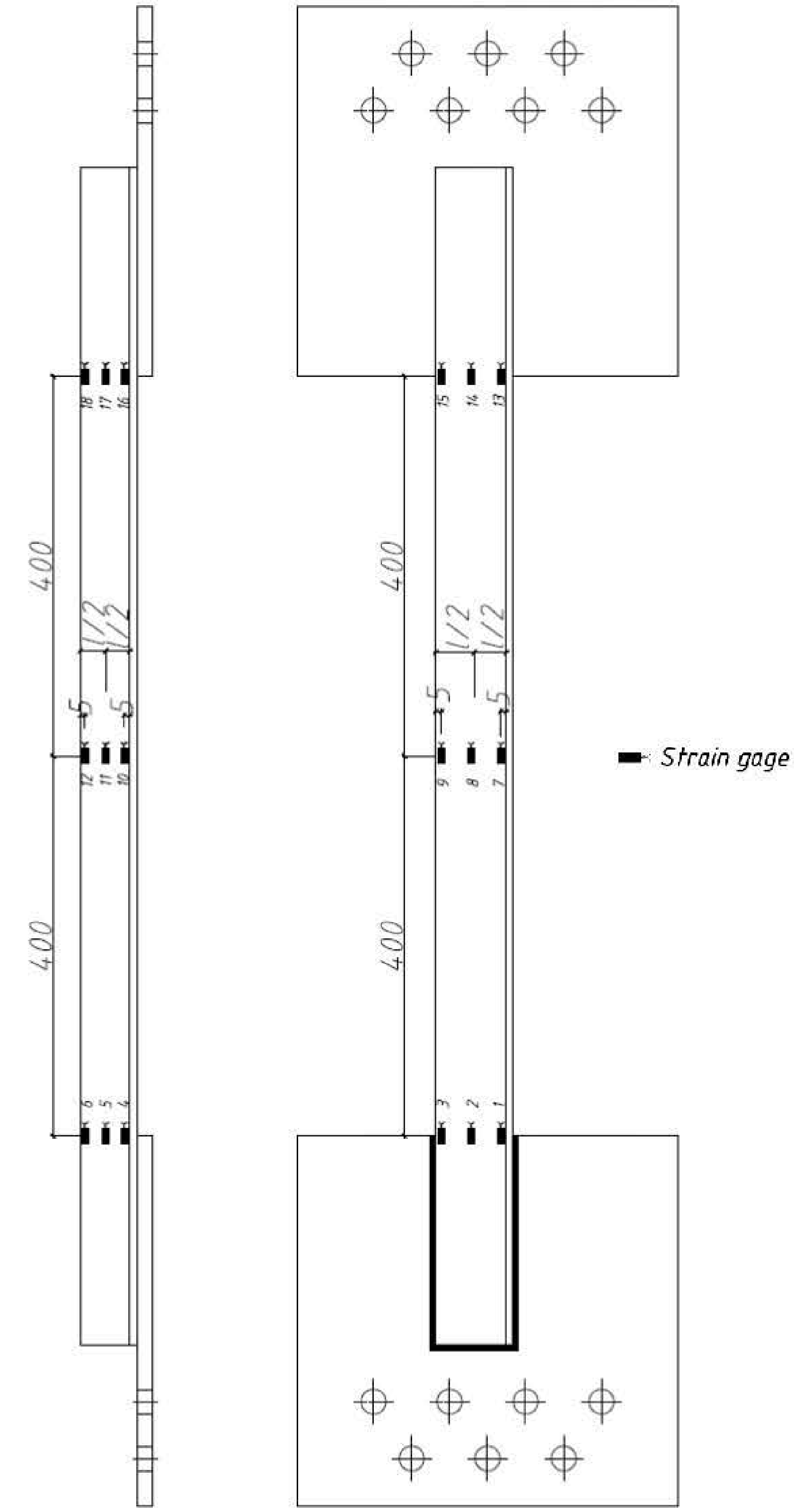

Figure 3.5 Layout of strain gages on the welded angle specimens

CHAPTER 4 TEST RESULTS AND DISCUSSION

4.1 TEST RESULTS

4.1.1 General observations

A total of 14 HSS and 4 NS tension members were tested. The test results, including the static ultimate loads, final elongation, and failure mode for the bolted and welded angle specimens, are listed in Tables 4.1 and 4.2, respectively. The nominal tensile capacity (i.e.$f_u A_n \ or \ f_u A_g$) and the test efficiency, which is defined as the ratio of the static ultimate load to the nominal capacity, are also presented in the tables. The test efficiency is generally considered a typical index of the shear lag effect. It is employed in the latter chapter to study the effect of each test parameter on the shear lag effect of the HSS specimens. The results of the tension coupon tests are shown in Table 4.3.

In the loading process, the gusset plates and the connected part of the angle were bent (Figure 4.1) until the loading line aligned with the centroidal axis of the angle. The angle specimens with a larger out-of-plane eccentricity bent more severely than the others. In particular, for the bolted angle specimens, the part of the angle near the innermost bolt gradually separated from the gusset plates during the bending process, thus creating a visible gap as shown in Figure 4.1.

The major failure mode of all the specimens was the net section fracture in the critical section regardless of the type of connection (bolted or welded) and the type of steel grade. For the bolted angle specimens, 8 out of 9 specimens failed at the critical section, except for specimen A2-60S which failed in a mixed way combining cracking of the critical section of the connected leg with shear failure of the welds connecting the two HSS plates forming the angle specimen. These two failure modes are illustrated in Figures 4.2 and 4.3. For the bolted angle specimens with critical section fracture failure, the crack started in the innermost bolt hole of the connected leg and then propagated to the edge of the connected leg and the outstanding leg. Finally, it penetrated the whole section. However, for specimen A2-60S, when the crack reached the heel of the angle, the weld was unable to stand the additional force from the cracking part of the connected leg, thus resulting in the shear failure of the welds. The fracture section consisted of the critical section of the connected leg and the shear plane of the weld. Although the fracture did not occur in the whole critical section, the ultimate load was treated as the net section capacity because the ultimate load was attained when the crack of the connected leg started to appear. The crack propagated so rapidly to form a whole section fracture that little increase of load was achieved.

7 of the 9 welded angle specimens exhibited fracture failure in the critical section near the inner edge of the longitudinal welds. The crack started at the toe of the connected leg. Thereafter, it propagated to the heel and finally ended in the outstanding toe. On the other hand, specimens C1-300L and D1-300L failed in the mid-length section of the angle. The fracture process was similar to the critical section fracture failure but occurred in different cross-sections. Normally, this type of failure mode indicates that sufficient ductility is achieved. Images of the two failure modes are shown in Figures 4.4 and 4.5.

4.1.2 Load deflection behaviour

The load–elongation curves of all the specimens are shown in Figures 4.6–4.9. The measured elongations were based on the displacement of the cross-head of the tension machine and thus included the deformations of all components. In general, the elongations of all the NS specimens were considerably larger than those of the HSS specimens because of the larger ductility of NS. All the specimens developed a linear load–elongation response in the initial stage. Thereafter, when the applied load reached approximately 60% of the ultimate load, the nonlinear response was observed when yielding occurred in the critical section. For the bolted angle specimens, a large yielding plateau was found in specimen B1-75L that was not observed in specimen B2-75S and all the HSS bolted angle specimens. As shown in Table 4.1, the total elongation and test efficiency of specimen B2-75S were significantly lower than expected and were even lower than those of the HSS specimens. With this observation, the test results of specimen B2-75S could include a certain experimental error. Thus, the load deflection behaviour of specimen B2-75S will be further investigated in the finite element analysis in Chapter 5. For the welded angle specimens, the two HSS specimens C1-300L and C1-380L also exhibited large inelastic deformation aside from the two NS specimens (D1-300L and D2-300S). This finding illustrates that HSS welded angles with long leg connections and a relatively long connection length also possess sufficient ductility and that the elongation of HSS welded angle specimens with a short leg connection is considerably lower because of a greater shear lag effect.

4.1.2 Strain distributions

Typical strain distributions of the bolted and the welded angle specimens are illustrated in Figures 4.10–4.15 and in Figures 4.16–4.21, respectively. The patterns of strain distributions of the bolted and welded angle specimens were almost identical, and the bolted angle specimens were taken as examples for discussion. Two sections were studied: the critical section (SG#1–SG#5) and the mid-length section (SG#6–SG#10). In general, the strain distributions of HSS and NS specimens followed the same pattern. As expected, yielding first occurred near the bolt hole of the critical section and then developed toward the edge of the connected leg and the unconnected leg. Non-uniform strain distributions were found in the critical section of the connected leg (SG#1 and SG#2) because of stress concentration around the bolt hole, whereas nearly uniform distributions were observed in the mid-length section of the connected leg (SG#6 and SG#7). The strains in the unconnected leg decreased from the heel to the outstanding toe because of the shear lag effect. Compressive strain was found near the edge of the unconnected leg (SG#5 and SG#10) in the early stage of loading because of the secondary bending effect. In the mid-length section, the strain (SG#10) gradually turned into tension as the load increased and the secondary bending effect diminished. However, the situation in the critical section varied depending on the connected leg. For instance, when the angle was connected with the long leg as shown in Figure 4.10, the compressive strain (SG#5) was relatively low, far below the yielding compressive strain. Subsequently, tensile strains exceeding the yield strain were developed in the final stage. However, when the angle was connected with the short leg as shown in Figure 4.12, the strains near the outstanding toe remained in compression throughout the entire loading process, even nearly reaching the compressive yield strain in the final stage. This difference was due to the fact that angles with a short leg connection had a higher out-of-plane eccentricity, thus resulting in a more severe secondary bending effect and shear lag effect.

4.2 DISCUSSION OF TEST RESULTS

The effects of all the main test parameters, including steel grade, connection length, and out-of-plane eccentricity, are investigated in this section. The test efficiencies of the angles are employed as the most important index to examine the shear lag effects. Load–elongation curves are also compared to demonstrate the influence of all parameters on the shear lag effect.

4.2.1 Effect of steel grade

As illustrated in Figures 4.6–4.9, except for the elongation of specimens A2-75S and B2-75S, the elongation of NS specimens was evidently larger than those of the corresponding HSS specimens because of the former's higher ductility. In addition, all NS specimens except specimen B2-75S exhibited an evident yielding plateau, whereas only welded angle specimens with a long leg connection (i.e., C1-300L and C1-380L) achieved a yielding plateau in HSS specimens,. This difference was mainly due to the different Y/T ratios combined with the shear lag effect. NS had a significantly lower Y/T ratio (0.65 of B1 series) than HSS (0.95 of A1 series). With this difference, for bolted angle specimens, the yielding of the full mid-length section of NS specimens could occur before the rupture of the net section, thus resulting in the yielding plateau. Conversely, for the HSS bolted angle specimens, the rupture of the net section occurred prior to the yielding of the mid-length section because of the high Y/T ratio. Therefore, no yielding plateau was found in all the HSS bolted angle specimens. In addition, for the HSS welded angle specimens, the nominal ultimate strength (i.e., $f_u A_g$) was only slightly higher than the nominal yield strength (i.e., $f_y A_g$) because of the high Y/T ratio. With the shear lag effect, the ultimate strength of the critical section was reduced and could be lower than the yielding strength of the mid-length section. Thus, the rupture of the critical section occurred before the yielding of the mid-length section. However, for HSS welded angle specimens with a long leg connection (i.e., C1-300L and C1-380L), the shear lag effect was negligible. As a result, the yielding of the mid-length section occurred before the rupture of the critical section, and a large yielding plateau was achieved.

As indicated in Tables 4.1 and 4.2, the test efficiencies of the NS specimens were generally higher than those of the HSS specimens. For the bolted angle specimens, the test efficiencies of specimens B1-75L and A1-75L were 1.01 and 0.95, respectively. For the welded angle specimens with a long leg connection, the test efficiencies of NS and HSS specimens were similar (1.02 for C1-300L and 1.00 for D1-300L). However, for the welded angle specimens with a short leg connection, the test efficiency of specimen D2-300S was 10% higher than that of specimen C2-300S. Although the test results of NS specimens were limited, a preliminary conclusion could be drawn from the comparisons. For the bolted and welded angle specimens with a long leg connection, the test efficiencies were not significantly affected by the steel grade. However, for the short leg connected specimens, the test efficiencies decreased with increased steel grade. A more detailed discussion and investigation are presented in the finite element analysis of the specimens in Chapter 5.

4.2.2 Effect of connection length

As shown in Figures 4.6 and 4.7, connection length had little effect on the shear lag effect regardless of the long or short leg connection for the bolted angle specimens. The test efficiency increased slightly with increased connection length. As presented in Table 4.1, the test efficiencies of specimens A1-60L, A1-75L, and A1-90L were 0.92, 0.95, and 0.96, respectively. For the short leg connected specimens, the test efficiencies of specimens A2-60S, A2-75S, and A2-90S were 0.70, 0.72, and 0.74, respectively. In addition, the elongations of the bolted angle specimens with different connection lengths were also found to be similar. These results were obtained on the condition that five bolts were used. Thus, varying the connection length by changing the bolt spacing may not illustrate the effect of connection length on the test efficiency when sufficient bolts are used. Five bolts were used to connect the bolted angle specimens to ensure that bolt shear failure would not occur prior to the net section fracture. Moreover, similar observations were presented by Kulak and Wu (1997); the connection length had a negligible effect on the shear lag effect of single angles when the number of bolts exceeded four. Therefore, a similar conclusion could be drawn as the shear lag effect of HSS bolted angles was not significantly affected by the connection length when five or more bolts were connected.

Similar observations on the effect of connection length were found in the welded angle specimens as illustrated in Table 4.2. For the long leg connections, specimen C1-300L achieved a test efficiency 5% higher than that of specimen C1-220L with an additional weld length of 80 mm. However, when the connection length exceeded 300 mm, a negligible difference of efficiency was found because the test efficiencies had already reached 1.00. As shown in Figure 4.8, specimens C1-300L and C1-380L exhibited a large inelastic deformation and achieved sufficient stress redistribution in the critical section. Therefore, the shear lag effect was significantly reduced, and no reduction in tensile capacity was found. For the short leg connected specimens, the test efficiency of specimen C2-380S with weld length of 380 mm was approximately

10% higher than those of specimens C2-220S and C2-300S with weld lengths of 220 and 300 mm, respectively. Although the test efficiencies of specimens C2-220S and C2-300S were similar (with C2-220S of 0.84 and C2-300S of 0.82), the overall test results of the welded angle specimens indicated that the test efficiencies increased with increased connection length.

4.2.3 Effect of out-of-plane eccentricity

The out-of-plane eccentricity of the test specimens was varied by changing the angle section size or by connecting the angles with either the long leg or the short leg. With respect to the bolted connection specimens, the effect of out-of-plane eccentricity on the shear lag effect was observed by studying the results of specimens A1-75L, A1-75S, and A2-75L with out-of-plane eccentricities of 15, 25, and 33 mm, respectively. As illustrated in Table 4.1, the test efficiencies decreased considerably as out-of-plane eccentricity increased. For example, with the same section size and connection length, the test efficiency of specimen A1-75L, which was connected by the long leg, was 20% higher than that of specimen A1-75S, which was connected by the short leg. The effect of out-of-plane eccentricity was also observed in the strain distributions. Similar conclusions were found for the welded angle specimens. High improvement in test efficiency was achieved as out-of-plane eccentricity decreased. Specimens C1-300L, C1-300S, and C2-300S had test efficiencies of 1.00, 0.89, and 0.82, respectively. Furthermore, the current test results of the bolted and welded angle specimens are generally similar to those observed in the previous studies of NS tension angles (Nelson, 1953; Chesson and Munse, 1963; Kulak and Wu, 1997; Zhu et al., 2009).

4.2.4 Evaluation of the $1-\bar{x}/L$ rule

The efficiencies of the bolted and welded angle test specimens predicted by the $1-\bar{x}/L$ rule are presented in Tables 4.1 and 4.2, respectively. The rule generally provided conservative predictions for all the NS specimens except for specimen B2-75S. On one hand, for the HSS bolted angle specimens, the $1-\bar{x}/L$ rule produced relatively accurate predictions of the efficiency for the long leg connected specimens. The test efficiency of specimen A1-60L was only 2% lower than the predicted value, and those of the other two specimens (A1-75L and A1-90L) were predicted accurately by the rule. However, the efficiencies of the bolted angle specimens with short leg connections were overestimated by the rule. The test efficiency-to-predicted efficiency ratio was 0.83 for specimen A1-75S and 0.81 for the other three A2 specimens, with a mean value of 0.82 and a coefficient of variation of only 0.012. Thus, similar overestimations were found when the efficiencies of HSS bolted angle specimens with short leg connections were predicted. On the other hand, the test efficiencies of all HSS welded angle specimens were accurately predicted by the rule, with a mean test-to-predicted ratio of 1.00 and a coefficient of variation of 0.016.

4.3 SUMMARY

The shear lag effect of HSS bolted and welded single angles were investigated by conducting full-scale tension tests of 14 HSS specimens and 4 NS specimens for comparison. The test parameters included steel grade, connection length, and out-of-plane eccentricity. The ultimate tensile capacities of all specimens were examined, and test efficiencies were employed to evaluate the shear lag effect. The test results indicated that the steel grade did not have a significant effect on the shear lag of the bolted and welded angle specimens with long leg connections. On the contrary, for the specimens with short leg connections, the shear lag effect became more severe with increased steel grade. The test results also showed that the shear lag effect was slightly affected by connection length and was strongly affected by out-of-plane eccentricity. The test efficiencies increased slightly with increasing connection length for the specimens with bolted connections when a sufficient number of bolts were used. For the welded angle specimens with long leg connections and relatively long connection length, full section capacity was achieved. In addition, the test efficiencies decreased considerably as the out-of-plane eccentricities increased for the bolted and welded angle specimens. Furthermore, the section efficiencies predicted by the $1 - \bar{x}/L$ rule were compared with the test efficiencies. Excellent agreement was found between the bolted angle specimens with long leg connections and all the welded angle specimens. However, the test efficiencies of the bolted angle specimens with short leg connections were generally overestimated by the rule.

Table 4.1 Test results of bolted angle specimens

Specimen	Ultimate load (kN)	Final elongation (mm)	$F_u A_n$ (kN)	Test Efficiency U_{Test}	Failure mode	$1-\bar{x}/L$ rule U_{Rule}	U_{Test}/U_{Rule}
A1-60L	632	21	687	0.92	C	0.94	0.98
A1-75L	656	22		0.95	C	0.95	1.00
A1-90L	660	21		0.96	C	0.96	1.00
A1-75S	542	18		0.79	C	0.92	0.83
A2-60S	590	19	846	0.70	C+W	0.86	0.81
A2-75S	613	17		0.72	C	0.89	0.81
A2-90S	625	17		0.74	C	0.91	0.81
B1-75L	395	36	392	1.01	C	0.95	1.06
B2-75S	311	15	483	0.64	C	0.89	0.72

Notes: "C" indicates critical section failure mode; "C+W" indicates the mixed failure mode combined critical section failure of connected leg with shear failure of weld.

Table 4.2 Test results of welded angle specimens

Specimen	Ultimate load (kN)	Final elongation (mm)	$F_u A_g$ (kN)	Test Efficiency U_{Test}	Failure mode	$1-\bar{x}/L$ rule U_{Rule}	U_{Test}/U_{Rule}
C1-220L	796	16	840	0.95	C	0.93	1.02
C1-300L	839	43		1.00	M	0.95	1.05
C1-380L	850	42		1.01	C	0.96	1.05
C1-300S	748	18		0.89	C	0.92	0.97
C2-220S	836	27	999	0.84	C	0.85	0.99
C2-300S	823	22		0.82	C	0.89	0.92
C2-380S	925	25		0.93	C	0.91	1.02
D1-300L	488	143	479	1.02	M	0.95	1.07
D2-300S	511	65	570	0.90	C	0.89	1.01

Notes: "C" indicates critical section failure; "M" indicates mid-length section failure.

Table 4.3 Summary of tension coupon test results

Material	Coupon No.	Elastic modulus (MPa)	Static yield stress (MPa)	Static ultimate stress (MPa)	Ultimate strain (%)
S690 (A/C series)	1	202915	773	810	6.9
	2	219020	753	795	7.0
	3	219911	755	790	6.0
	4	219651	764	800	6.7
	Mean	215374	761	798	6.7
S275 (B/D series)	1	219450	296	462	20.7
	2	218443	290	445	20.8
	3	215620	289	463	20.6
	4	219562	293	442	20.6
	Mean	218268	292	453	20.7

Figure 4.1 Typical deformed mode of all specimens

Figure 4.2 Typical critical section failure mode of bolted angle specimens

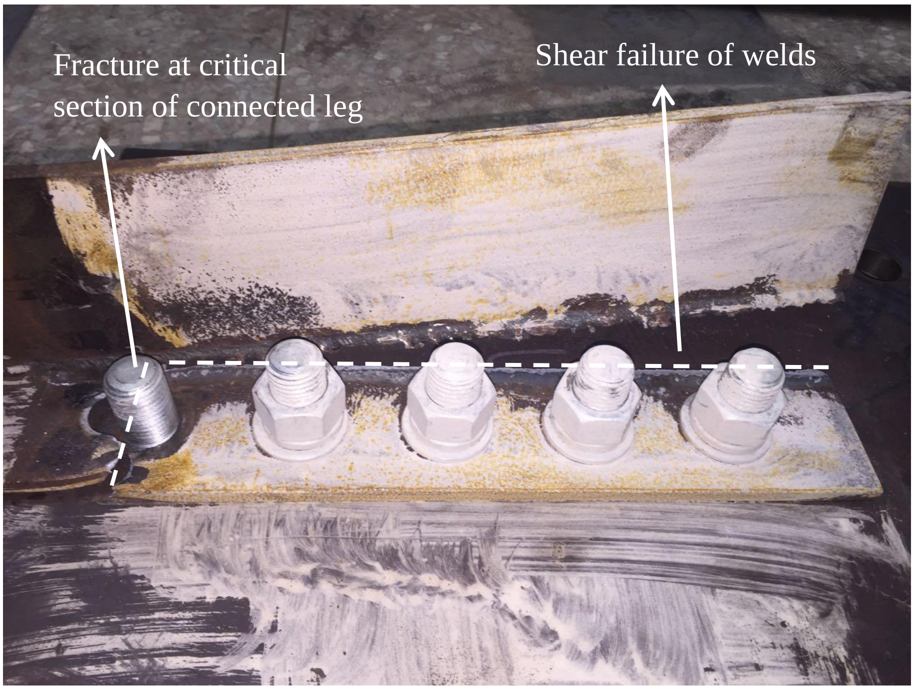

Figure 4.3 Typical mixed failure mode of A2-60S

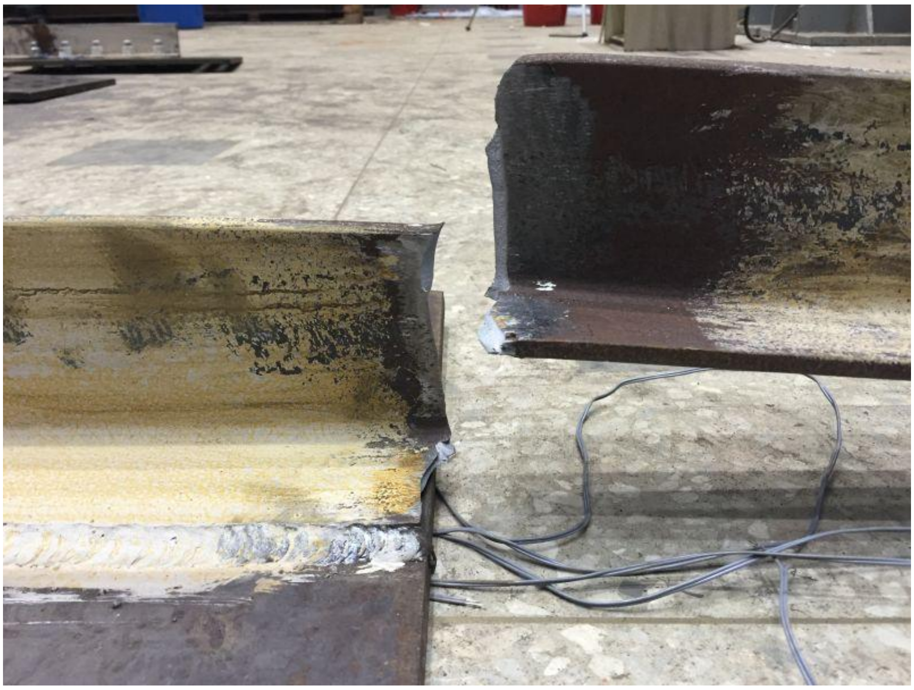

Figure 4.4 Typical critical section failure mode of welded angle specimens

Figure 4.5 Typical mid-length section failure mode of welded angle specimens

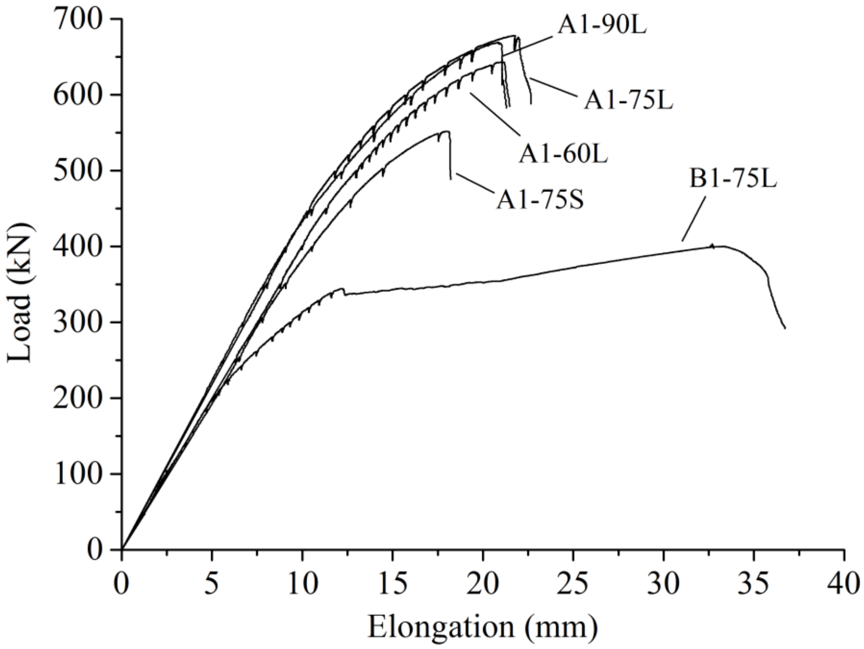

Figure 4.6 Load-elongation curves of bolted specimen A1/B1 series

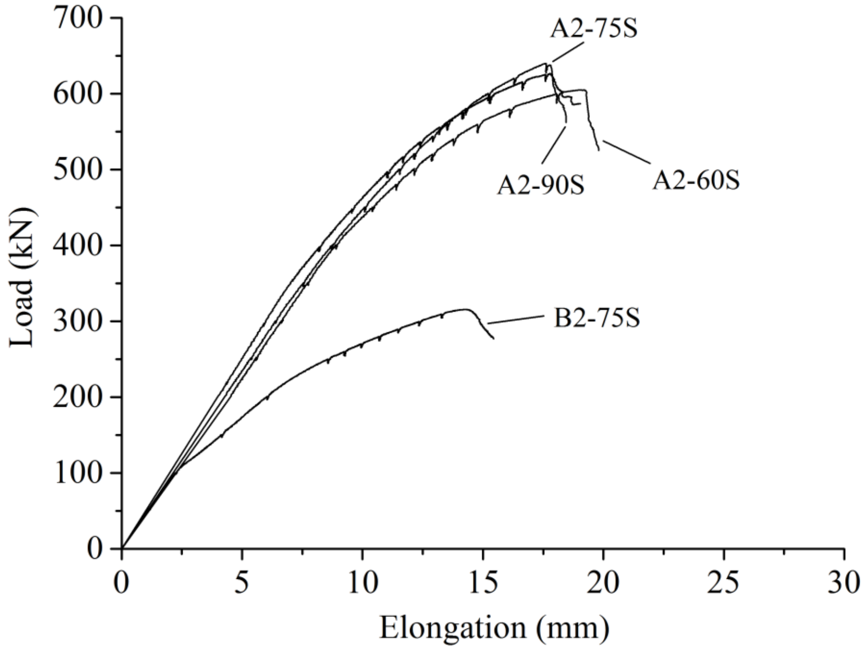

Figure 4.7 Load-elongation curves of bolted specimen A2/B2 series

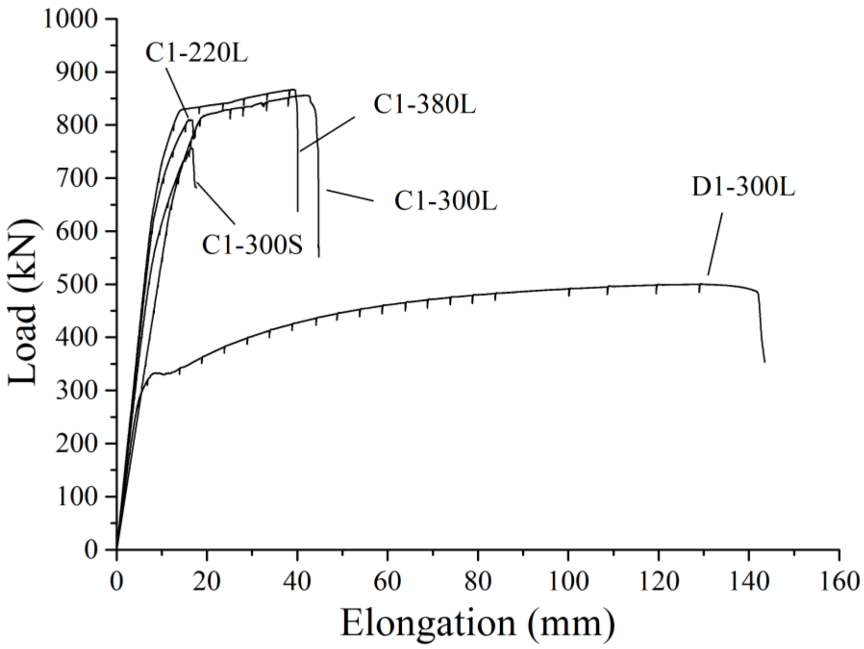

Figure 4.8 Load-elongation curves of welded specimen C1/D1 series

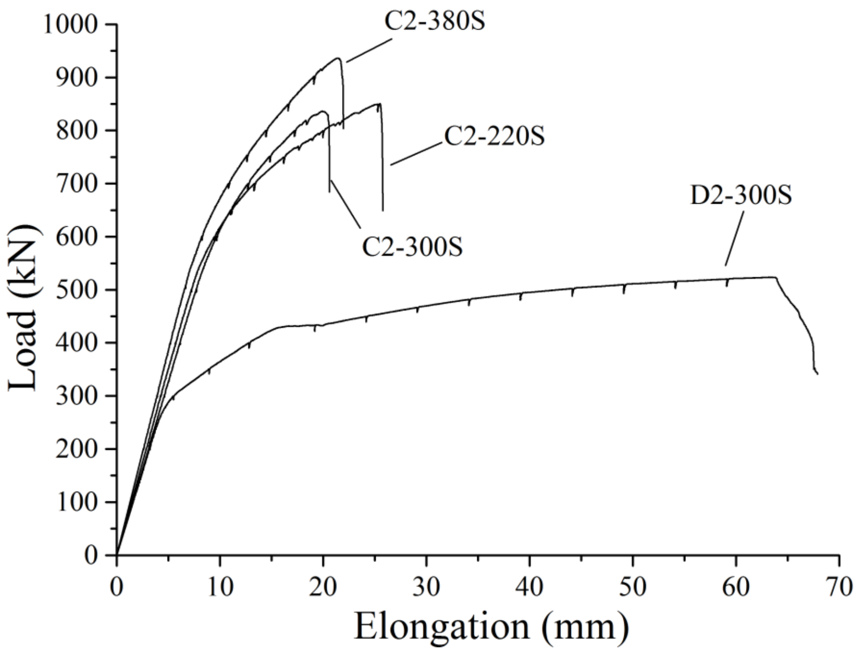

Figure 4.9 Load-elongation curves of welded specimen C2/D2 series

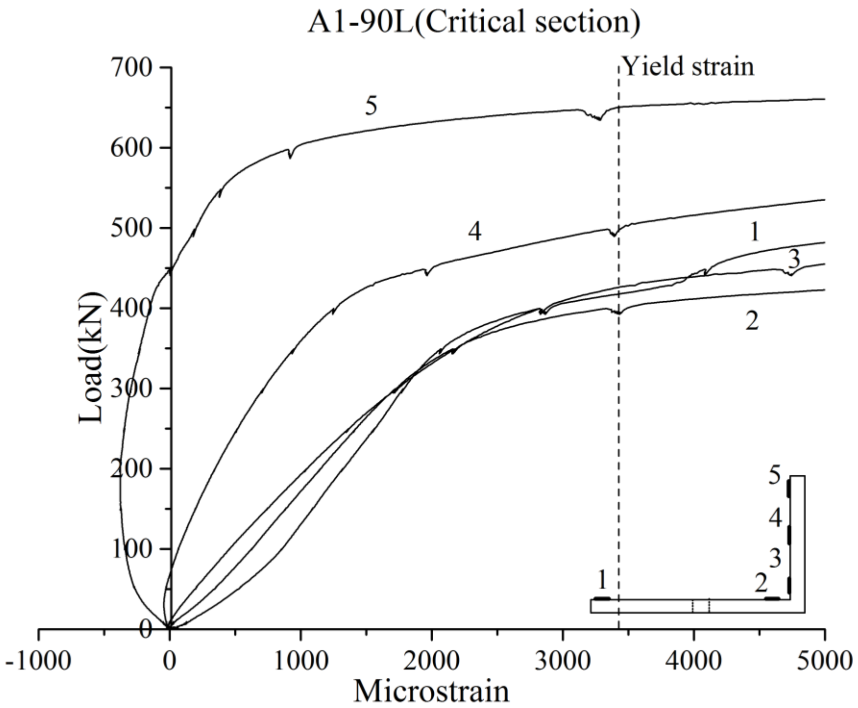

Figure 4.10 Strain distribution of critical section of bolted specimen A1-90L

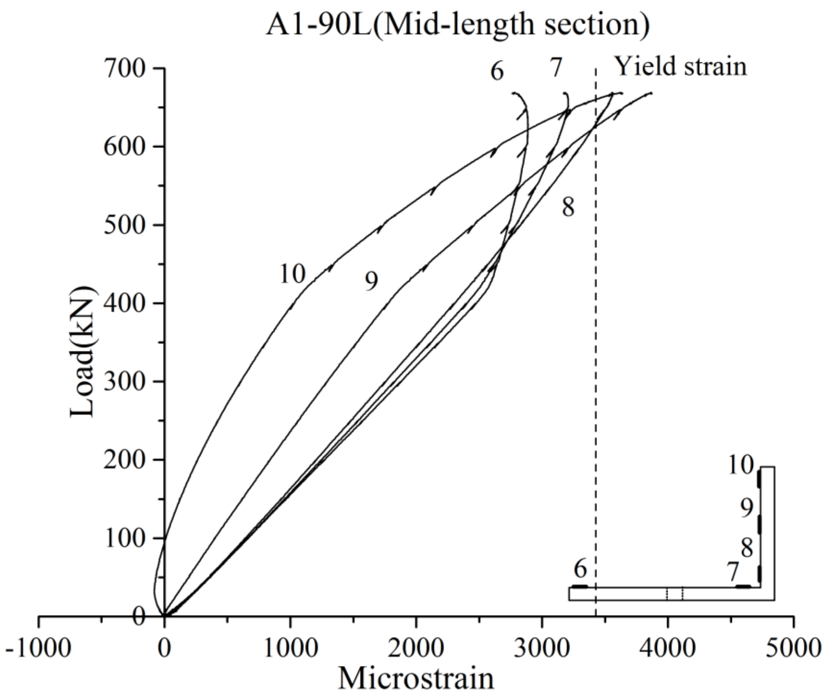

Figure 4.11 Strain distribution of mid-length section of bolted specimen A1-90L

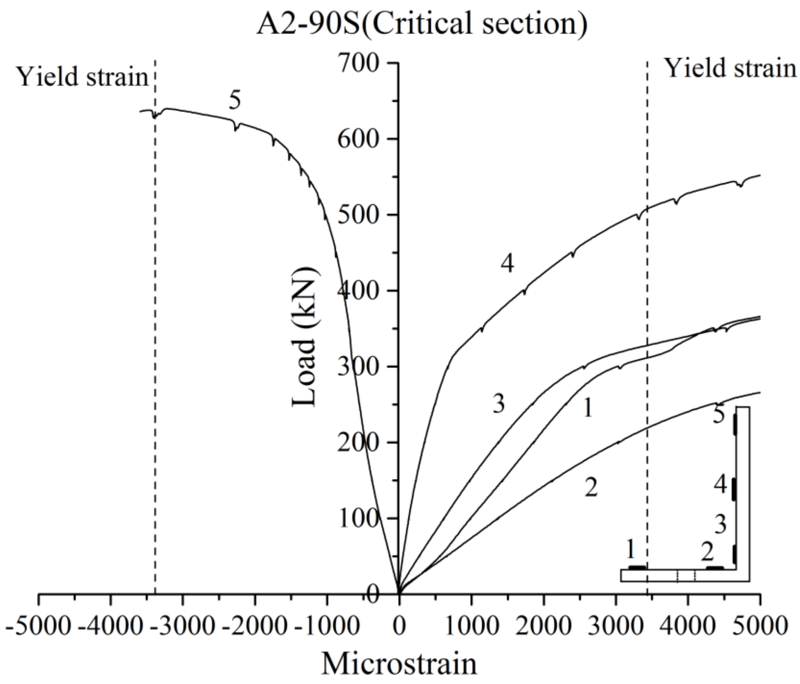

Figure 4.12 Strain distribution of critical section of bolted specimen A2-90S

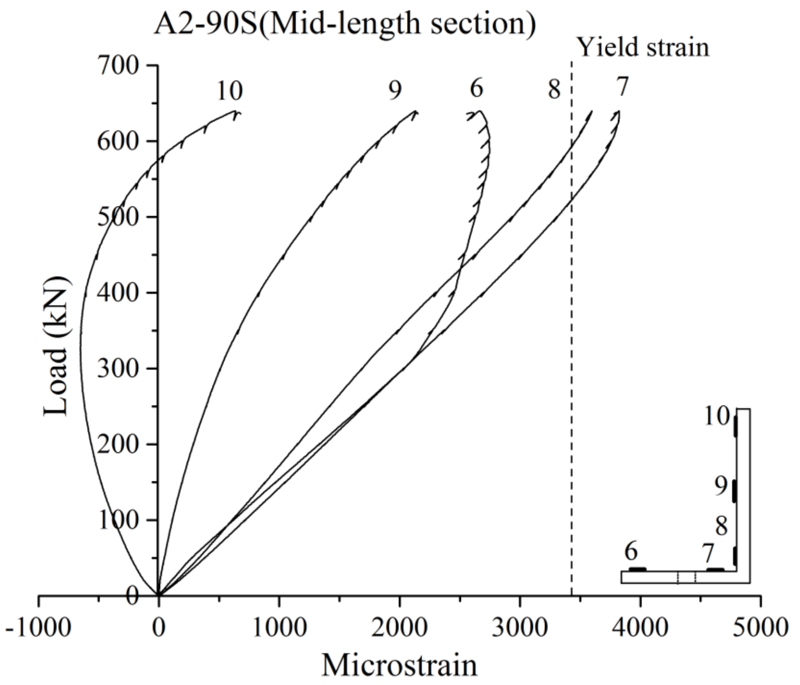

Figure 4.13 Strain distribution of mid-length section of bolted specimen A2-90S

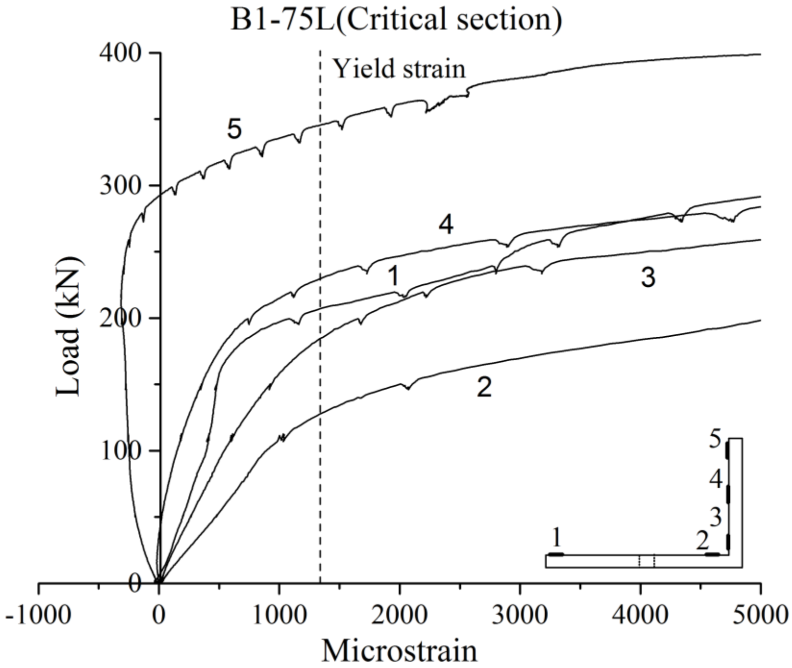

Figure 4.14 Strain distribution of critical section of bolted specimen B1-75L

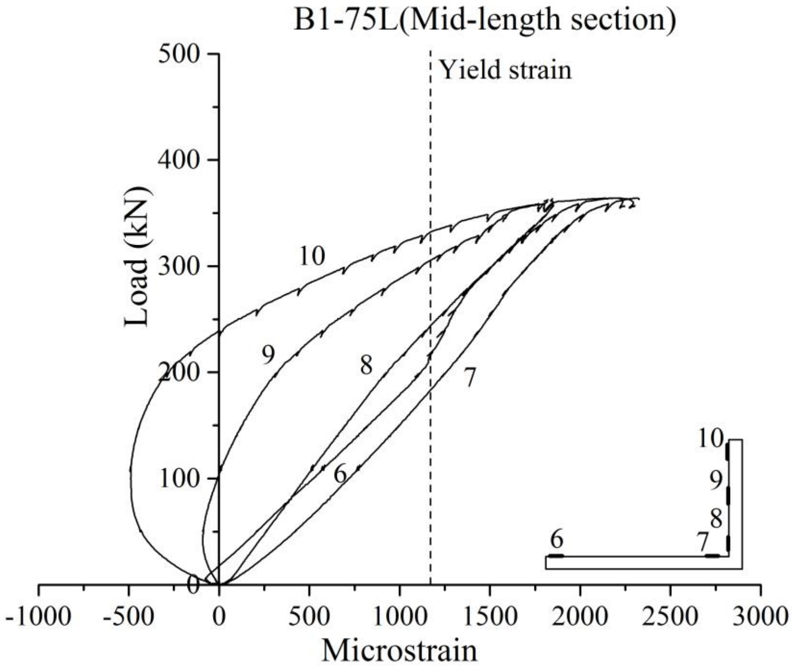

Figure 4.15 Strain distribution of mid-length section of bolted specimen B1-75L

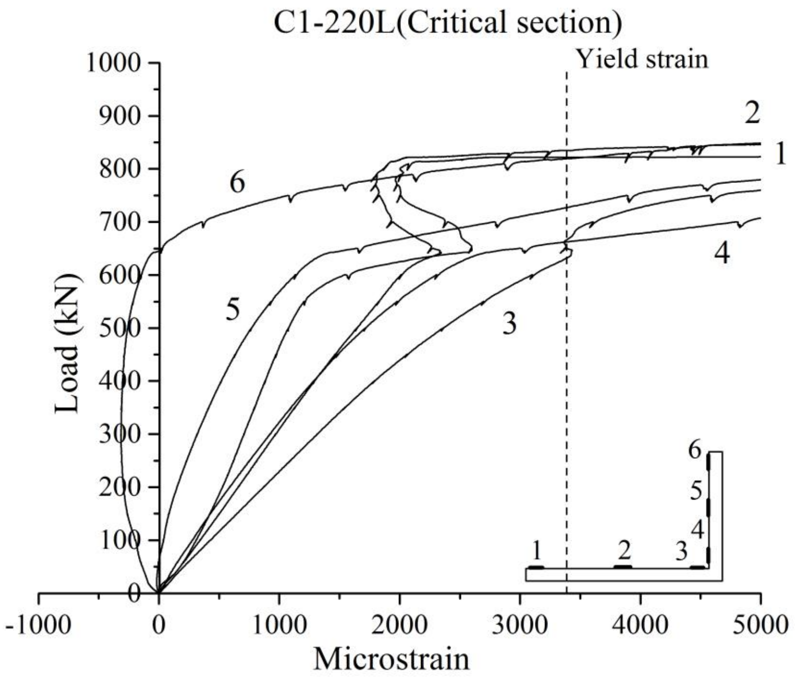

Figure 4.16 Strain distribution of critical section of welded specimen C1-220L

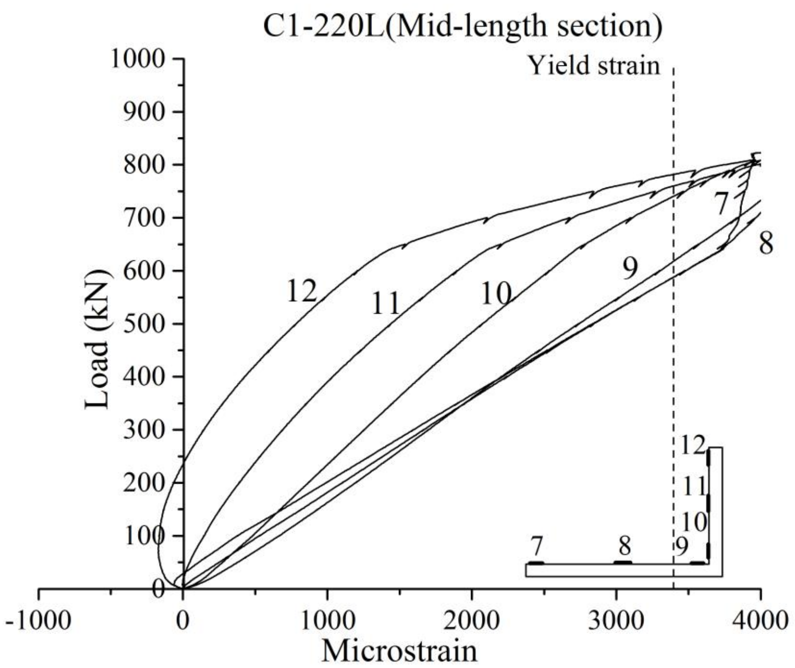

Figure 4.17 Strain distribution of mid-length section of welded specimen C1-220L

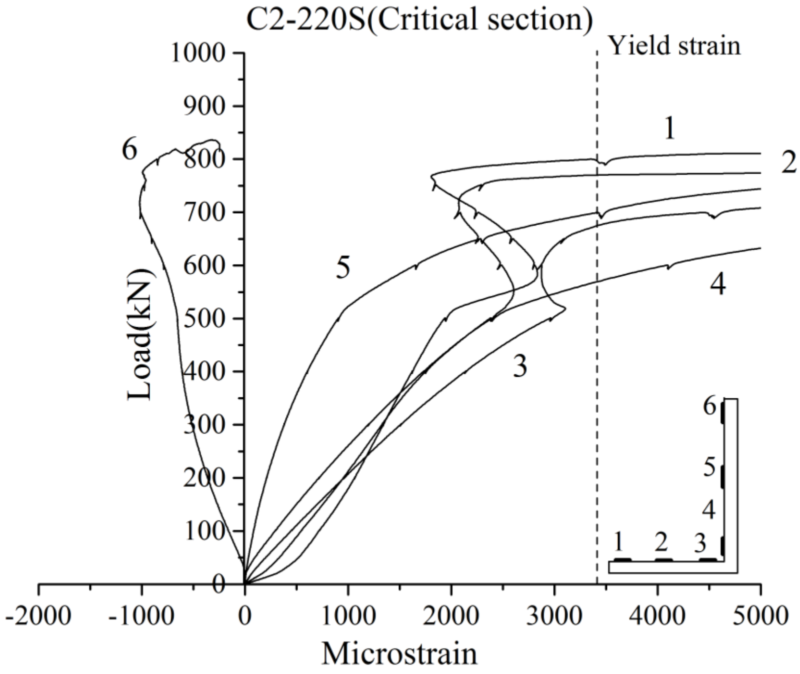

Figure 4.18 Strain distribution of critical section of welded specimen C2-220S

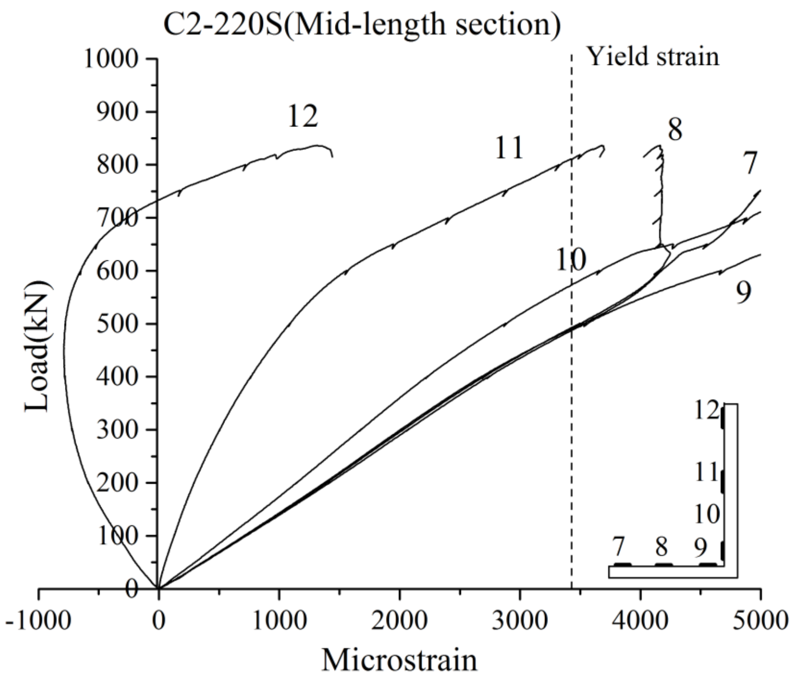

Figure 4.19 Strain distribution of mid-length section of welded specimen C2-220S

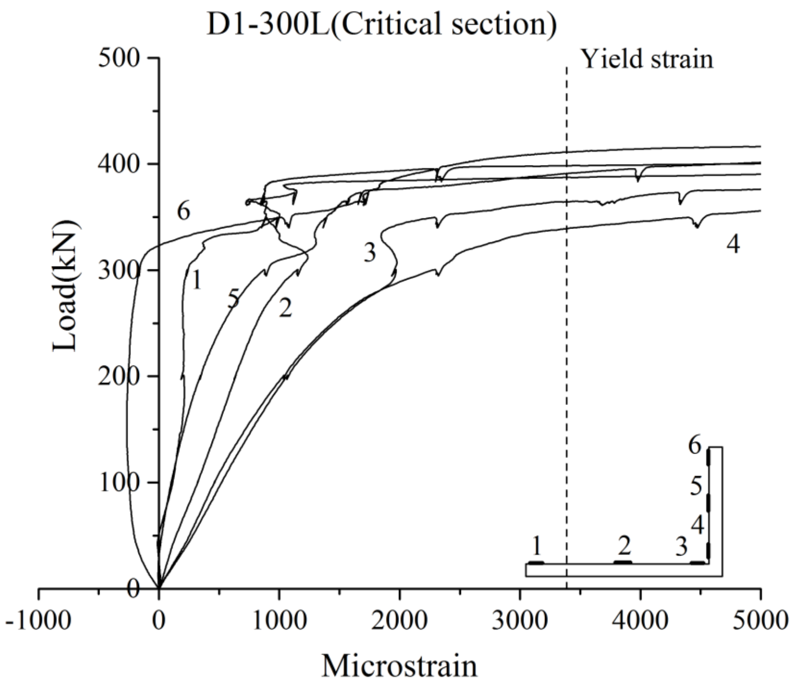

Figure 4.20 Strain distribution of critical section of welded specimen D1-300L

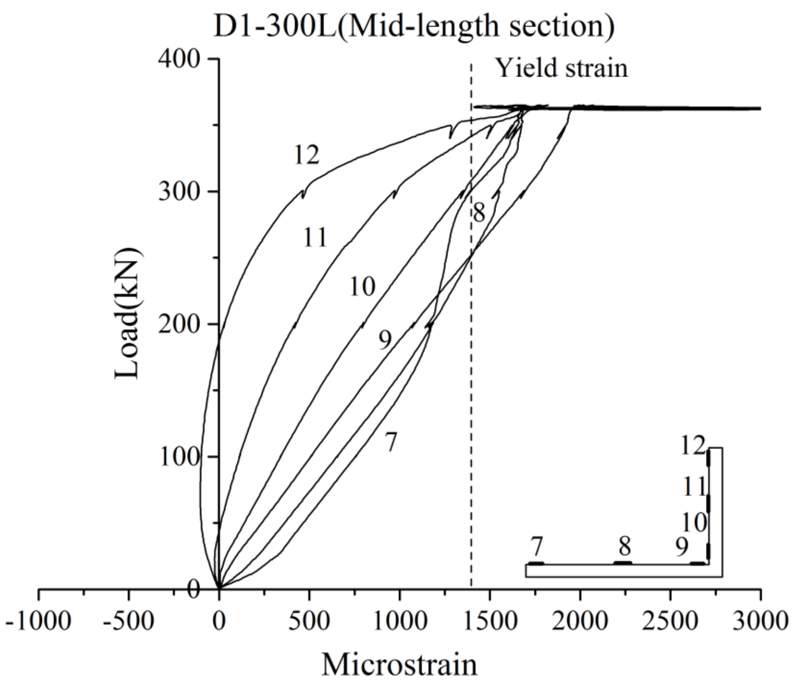

Figure 4.21 Strain distribution of mid-length section of welded specimen D1-300L

CHAPTER 5 FINITE ELEMENT ANALYSIS

5.1 GENERAL

Finite element (FE) models were established to analyze the shear lag effect of HSS single angle tension members. The commercial FE programme ABAQUS version 6.12 (Hibbit et al., 2012) was employed. This chapter first describes the details of the FE model, which consists of element selection, boundary conditions, contact simulation, and material property models. Subsequently, the numerical results are compared with the corresponding test results to validate the model. Finally, a parametric study with an enhanced range of test parameters is conducted using the verified model.

5.2 NUMERICAL MODEL

5.2.1 Element selection

Normally, two types of elements are available to simulate tension members, namely, shell elements and solid elements. Both element types have been used in many studies involving the modeling of tension members (Kulak et al., 1997; Zhu et al., 2009; Može and Beg, 2010). On one hand, using shell elements avoids the possible converging problems caused by the complex contact between the bolts and the bolt holes under an eccentric loading. The bolts are simply omitted when the model is constructed with shell elements. Instead of a hard contact, the interactions among the gusset plate, the bolts, and the angle are simplified to a direct interaction between the gusset plate and the angle by coupling the movements of the bolt holes in the angle with the corresponding bolt holes in the gusset plate. This node-to-node coupling becomes significantly easier by employing shell elements than solid elements. With this approach, converging problems are avoided, and computing time can be reduced correspondingly. However, the calculated stresses around the bolt holes may be less accurate because of the simplification of the bolt–bolt hole contact. On the other hand, solid elements can provide a full analysis that considers the effects of all pairs of contact, thus producing accurate results. Thus, solid elements were selected to build the FE models in this study. The possible converging problems were resolved by refining the mesh grid and adjusting the mesh sizes by trial and error.

For the solid elements, the arrangement of integration points includes either full integration or reduced integration. Generally, elements with full integration are not recommended when the models are subject to evident bending moment because they will result in the shear locking effect, which can make the model stiffer than it should be. This effect can be avoided by using solid elements with reduced integration. Among these elements, C3D20R and C3D8R have been frequently used. Furthermore, a quadratic element with reduced integration such as C3D20R was not chosen in this study because this type of element could not simulate the hard contact (Hibbit et al., 2012). Thus, a linear solid element with reduced integration C3D8R was used in this model. However, the major concern of C3D8R is its hourglass effect. Because there is only one integration point in element C3D8R, it is not able to provide bending resistance. This problem is resolved in ABAQUS by introducing a built-in "hourglass stiffness," and this approach works better with a finer mesh grid. Generally, the hourglass effect can be avoided when at least four elements are meshed in the direction of thickness; this approach was adopted in this study. In addition, the ratio of the artificial strain energy (ALLAE) to the internal energy (ALLIE) should be maintained under 1% to avoid overuse of hourglass stiffness, which may lead to inaccurate results (Hibbit et al. 2012). The above discussion indicates that the 3D, eight-node linear brick, reduced integration, and hourglass control elements (C3D8R) were used to model the angle, gusset plates, bolts, and welds as shown in Figure 5.1.

5.2.2 Boundary conditions

The typical models of the bolted and welded angle specimens are shown in Figures

5.2 and 5.3, respectively. Given symmetry, only the half scale of each specimen was modeled. At the mid-length of each specimen, translational degree of freedom (DOF) in the x-direction and rotational DOF on the y and z axes were constrained following the axis–symmetry characteristic. The leading edge of the gusset plate was restrained in all directions except the longitudinal. A longitudinal uniform displacement was applied on the leading edge as the axial load. The end fixtures and the bolt holes of the gusset plates were not modeled for simplification. Thus, the load was not transferred through the seven bolts at each end of the gusset plate as observed in the tests. This simplification was acceptable because the gusset plate was designed to maintain within the elastic range, and the stress distribution in the gusset plate near the end of the angle should be uniform in the tests. In addition, the main elongation of the specimen occurred in the plastic region of the angle, and it was over 100 times the elastic elongation of the gusset plates.

As the extension obtained in the test was the total of the elongation of the specimen and the elastic deformation of the end fixtures, “spring” elements were attached to the specimens in the mid-length section to simulate the elastic deformation of the end fixtures. The stiffness of the spring was determined by calibrating the initial stiffness of the test load deflection curves.

5.2.2 Contact simulation

For both bolted and welded connections, the global contact interaction with normal behaviour of “hard” contact and tangential behaviour of “penalty” friction formulation was prescribed among all parts. “Hard” contact means that no penetration was allowed on each contact surface. A value of 0.25 was adopted as the friction coefficient, which was the measured average nominal coefficient of various steels (Vasarhelyi and Chiang, 1967).

For the bolted connections, certain simplifications were introduced in the FE models. The length of the bolt shank was designed as the sum of the thickness of the angle and the gusset plate. The part of the bolt outside the nut was omitted. The bolt shank, the nut, and the washer were created as a unity, thereby indicating that the interaction among these parts was not considered. Preload was applied on each bolt at the first step of loading to ensure tight contact (snug-tight during testing). The quantity of the preload was set to 70% of the bolt's tensile strength. A 2 mm clearance was present between each bolt shank and bolt hole. Prior to loading, the bolts were made to contact with the bolt holes at the beginning to eliminate any slips. This approach was taken to prevent any undesired computational error that could occur easily the moment the bolt shank bore on the bolt hole. In addition, slips between the bolt shanks and the bolt holes were also eliminated by pre-loading in the tests.

In the welded connection, welds were treated as a rigid connection between the angle and the gusset plates. No displacement or rotation was allowed on the contact surface. Thus, the "tie" constraints in ABAQUS were prescribed among all weld–gusset plate and weld–angle contact pairs. The "tie" constraints were normally used to establish a rigid connection between every pair of nodes from two contact surfaces. All the movements in the six DOFs were kept identical between each pair.

5.2.3 Material model

An incremental isotropic-hardening elastic–plastic material model with the von Mises yield criterion was used. The engineering stress–strain curve obtained from the coupon tests was approximated by a polygonal stress–strain curve, which is a reasonable simplification for the input material data. Subsequently, the engineering stress and strain was converted to true stress and true strain using Eqns. 5.1 and 5.2 as follows:

$$\sigma_{true} = \sigma_{eng}(1 + \varepsilon_{eng}) \quad (5.1)$$

$$\varepsilon_{true}^{p} = \ln(1 + \varepsilon_{eng}) - \frac{\sigma_{true}}{E} \quad (5.2)$$

where σ_{true} is the true stress, σ_{eng} is the engineering stress, ε_{true}^{p} is the true plastic strain and ε_{eng} is the engineering strain.

These equations can be easily determined on the basis of the definition of true stress and true strain as shown in Eqns. 5.3 and 5.4, respectively, along with the fact that the volume of steel remains constant during the plastic stage.

$$\sigma_{true} = \frac{F}{A} \quad (5.3)$$

$$\varepsilon_{true} = \int_{L_0}^{L} \frac{dL}{L} = \ln\left(\frac{L}{L_0}\right) = \ln(\frac{A_0}{A}) \quad (5.4)$$

Where F is the current applied load, A is the current cross-section area, A_0 is the original cross-section area, L is the current length and L_0 is the original length.

However, Eqns. 5.1 and 5.2 are only applicable when uniform strain occurs along the length of the tension coupon, which corresponds to the stage prior to the necking of the coupon (Dowling, 1993). Normally, necking occurs immediately after the ultimate engineering strength is reached. During the necking stage, a large localized deformation occurs in the necking region, and the remaining part remains almost undeformed. Thus, the true stress–strain cannot be obtained directly from Eqns. 5.1 and 5.2 because the elongation of the coupon is no longer uniform after the peak load. To account for the effect of necking of the coupon on the true stress–strain behaviour of the material, the method based on the research of Cheng et al. (1998) and Li (2014) was adopted in this study. The true stress–strain relationship before the onset of necking was obtained directly from Eqns. 5.1 and 5.2. Subsequently, the true stress–strain curve between the onset of necking and the fracture was simplified as a linear relationship. Furthermore, the true stress–strain at fracture could be calculated on the basis of the definition of true stress and true strain using Eqns. 5.5 and 5.6.

$$\sigma_{true,f} = \frac{P_f}{A_f} \tag{5.5}$$

$$\varepsilon_{true,f} = \ln\frac{A_0}{A_f} \tag{5.6}$$

Where $\sigma_{true,f}$ is the true stress at fracture, $\varepsilon_{true,f}$ is the true strain at fracture, P_f is the applied load at fracture and A_f is the cross-section area at the necking region at fracture.

The complete true stress–strain data of steel S690 and S275 used in the model are presented in Table 5.1 and Figure 5.4. To verify the material model, numerical simulations of the standard coupon tests, which used the proposed true stress–strain curves, were conducted. The numerical engineering stress–strain curves of steel S690 and S275 were compared with the experimental engineering stress–strain curves as shown in Figures 5.5 and 5.6, respectively. Good agreement was observed in the comparison. According to Cheng et al. (1998), the real fracture strain of the material should be less than the complete fracture strain of the whole coupon because it was reasonable to assume that the fracture of a certain point in the necking area occurs before the complete fracture of the whole coupon. Thus, the fracture strain adopted in the model was less than the experimental fracture strain.

To define the fracture, the functions “damage initial” and “damage evolution” were used. The damage was initiated once the fracture strain was reached. The “damage evolution” indicated how the von Mises stress of elements decreased from top to zero when fracture strain was attained, which in this model was a linear reduction with the fracture element elongated by 0.0001 mm more. This mean that once the fracture strain was reached, the stress of elements declined immediately to zero, and then the elements were removed. The peak point of the numerical load–elongation curve was reached when one element was removed. The curve turned to the descending branch as more elements in the critical section fractured. However, the procedure in this model, which employs the static method, would stop at the peak point because converging was difficult when one of the elements was removed. By contrast, the procedure with the dynamic method was able to simulate the descending curve because the converging problem was avoided. However, the computing time would also substantially be increased. A comparison of the numerical load–elongation curves that use the static and dynamic methods is presented in Figure 5.7 to demonstrate that the descending curve could be modelled through this material model and that the peak point could be obtained using static method. To save computing time and as the descending part of the load–elongation curve was not crucial for this research study, all specimens were modeled using the static method.

5.3 FINITE ELEMENT RESULTS

5.3.1 Comparison of experimental and numerical results

The comparison between experimental and numerical load–elongation curves is illustrated in Figures 5.8 and 5.9 for the bolted and welded angle specimens, respectively. All the numerical load–deflection curves except specimen B2-75S were in good agreement with the experimental ones. Furthermore, for specimen B2-75S, the numerical curve indicated a good agreement with the experimental one until the fracture of the specimen. Afterwards, the experimental load began to descend, whereas the numerical load continued to ascend. The final tensile capacity and elongation of specimen B2-75S based on FE analysis were much larger than those obtained in the experiment. This discrepancy also verified the assumption that specimen B2-75S fractured prematurely because of certain experimental errors that could not be identified from the test results and observation. Furthermore, the comparisons between the test and the FEM efficiencies are presented in Tables 5.2 and 5.3 for the bolted and welded angle specimens, respectively. The ratios of the test load to the FEM load of the HSS bolted angle specimens ranged from 0.95 to 0.97

with a mean value of 0.96 and a coefficient of variation of 0.01. For the HSS welded angle specimens, the ratio ranged from 0.99 to 1.03 with a mean value of 1.01 and a coefficient of variation of 0.02. Given that both the mean values were close to 1.00 and that the coefficients of variation were relatively small, the model provided markedly accurate predictions of the ultimate capacities. In addition, all bolted and welded angle specimens in FEM were found to have a fracture in the critical section, consistent with the observations in the test. The typical comparisons of failure modes between the test and the FEM are shown in Figures 5.10 and 5.11 for the bolted and welded angle specimens, respectively. In addition, the typical fracture process of the bolted angle specimens is illustrated in Figure 5.12, which shows the process from elastic response all the way to fracture in the critical section. Moreover, the strain distributions were examined for further verification. The typical comparisons of strain distributions are shown in Figure 5.13. Strains recorded in the critical section and in the mid-length section at the applied load of 100 kN and 200 kN (both were within the elastic range of all load–elongation curves) were compared, and a reasonable agreement was achieved. The largest difference was found from the strain gage readings around the bolt hole. A likely reason for this result is the complex interaction between the bolt and the bolt hole. Nevertheless, this difference could gradually diminish when the region entered the plastic range. Therefore, the predictions of the ultimate load would be unaffected. Thus, based on the above, the FE model used was capable of predicting the tensile capacities of the HSS bolted and welded single angles. In the following chapter, the results of the parametric study using the validated FE model to further investigate the shear lag effect on the tensile strength of HSS angles are presented.

5.3.2 Parametric study

As previously described, the $1-\bar{x}/L$ rule was able to accurately predict the tensile capacities of the HSS welded angle specimens, but it overestimated the tensile capacities of the HSS bolted angle specimens with a short leg connection. Thus, to further examine the applicability of the $1-\bar{x}/L$ rule to the HSS bolted angle specimens, a parametric study with an extended range of parameters was conducted using the validated finite element model. Given that no evident overestimation was found in predicting the HSS welded angle specimens, only the bolted angle specimens were included in the parametric study. A total of 39 bolted single angles were simulated as shown in Table 5.4. The main parameter was the steel grade, including S275, S690, and S960 steels. In particular, the S960 steel, which generally has an even smaller ductility than the S690 steel, was added in the parametric study to enrich the range of ductility of steels. Thus, more extensive data on the shear lag effect of specimens made of steels with a broader range of ductility were obtained. In addition, the relationship between the shear lag effect and the steel grade (or the ductility of steel) was better explored. The applicability of the $1-\bar{x}/L$ rule to specimens with an enhanced range of steel grades was examined. The true stress–strain data of all steels are presented in Table 5.1 and Figure 5.4. In addition, the effect of connection length and out-of-plane eccentricity on the shear lag effect of specimens made of HSS was also examined. Notably, the variation in connection length was arranged by a constant bolt spacing of 75 mm and different numbers of bolts of 3, 4, and 5. The variation of out-of-plane eccentricity was arranged by a constant length of the connected leg of 75 mm and different lengths of the unconnected leg of 50, 75, and 100 mm with an out-of-plane eccentricity of 13, 22, and 31 mm, respectively. These values also represented the cases of long leg, equal leg, and short leg connection, respectively.

5.3.2.1 Effect of steel grade

The effect of steel grade on the shear lag effect is illustrated in Figure 5.14. The figure presents nine series of data that are a combination of three different connection lengths and three different out-of-plane eccentricities. When the angles were connected by the long leg, all the efficiencies of the specimens reached a high level of over 0.95, thereby indicating that the shear lag effect was almost negligible. The difference among the specimens with different steel grades was observed to be small. The efficiencies of specimens made of NS were even lower than those of the specimens made of HSS. This result was contrary to the expectations that the former should be higher. A possible reason is that when the long leg was connected, the length of the unconnected leg was relatively so short that the load could be easily mobilized to the full section of the unconnected leg before fracture of the connected leg regardless of the ductility of the material. Thus, for both HSS and NS specimens, the full section of unconnected leg could achieve its yield strength. As HSS possesses a much higher Y/T ratio than does NS, the ultimate strength of HSS specimens may be closer to its nominal tensile capacity. Therefore, the section efficiency of HSS specimens may be correspondingly higher than that of the NS specimens.

However, for the cases of equal leg and short leg connections, the efficiencies were found to decrease with decreasing ductility. For angles with equal leg connections, the efficiencies were lowered by a value of 0.02 from grade S275 to S690 steel and 0.06 from grade S275 to S960 steel. Although the difference was not evident, the trend still showed the effect of steel grade on the shear lag effect. Furthermore, for angles with short leg connections, the efficiencies decreased more significantly by a value of 0.08 from grade S275 to S690 steel and 0.10 from S275 to S960 steel. Therefore, the shear lag effect became more severe for HSS angles with either equal or short leg connections.

5.3.2.2 Effect of connection length

The effect of connection length on the shear lag effect is illustrated in Figure 5.15. Nine series of data that consist of three different steel grades and three different out-of-plane eccentricities are also presented. For specimens with any of the three steel grades, the efficiencies were not significantly affected by the connection length for long leg connections. The reason is that the efficiencies were so high (close to 1.00) that increases in the connection length could not result in a significant difference in the efficiency. However, for angles with equal leg connections, an evident improvement of efficiency was found as the connection length increased. The average increase in efficiency by adding one bolt (75 mm for connection length) was roughly 0.03 for angles made of S275 steel and 0.05 for angles made of both S690 and S960 steels. Moreover, similar to equal leg connections, the average increase in efficiency for the short leg connected angles by adding one bolt was approximately 0.05 for specimens with all steel grades. All of these findings matched with the experimental results discussed in Chapter 4, in which the shear lag effect of bolted angles made of all steel grades was not evidently affected by connection length when a long leg was connected but was moderately affected when equal or short leg was connected.

5.3.2.3 Effect of out-of-plane eccentricity

The effect of out-of-plane eccentricity on the shear lag effect is presented in Figure 5.16. Similarly, nine series of data consisting of three different steel grades and three different connection lengths are plotted. The figure indicates that the efficiencies of all the specimens were greatly affected by out-of-plane eccentricity. The decrease in efficiency from a long leg connection to a short leg connection (as eccentricity increased from 13 mm to 31 mm) was more than 0.20 for specimens made of both S690 and S960 steel. The largest decrease in efficiency could even reach nearly 0.30. Taking specimens M2-L-3, M2-E-3, and M2-S-3 as an example, which were all made of S690 steel and connected with three bolts, the efficiency of M2-L-3 was 0.30 higher than that of M2-S-3. For specimens made of S275 steel, the decrease in efficiency ranged from 0.10 to 0.20 for different connection lengths. These findings also agreed with the patterns of the test results illustrated in Chapter 4.

5.3.2.6 Evaluation of $1-\bar{x}/L$ rule

The ratios of FEM efficiency (U_{FEM}) to the predicted efficiency by the $1-\bar{x}/L$ rule (U_{RULE}) of all the angles examined in the parametric study are plotted in Figure 5.17. As the connection type varied from a long leg connection to a short leg connection, the ratios tended to decrease, thus indicating that the predictions by the $1-\bar{x}/L$ rule tended to be less conservative. For the angles with long leg connections, the U_{FEM}/U_{RULE} ratios for angles made of all three steel grades were all larger than or close to 1.00, thus indicating that the predictions were generally conservative. However, for the angles with equal or short leg connections, the changes in the U_{FEM}/U_{RULE} ratio varied with different steel grades. For angles made of S275 steel, the U_{FEM}/U_{RULE} ratios remained close to 1.00, with a mean value of 0.98 and 0.95 for equal and short leg connections, respectively. However, the U_{FEM}/U_{RULE} ratios of angles made of S690 and S960 steels with equal and short leg connections ranged from 0.98 to 0.79 and from 0.94 to 0.77, respectively. Therefore, the predictions by $1-\bar{x}/L$ rule tended to be un-conservative for HSS specimens with a relatively high out-of-plane eccentricity (equal or short leg connections). Thus, a recommendation for a revised equation is strongly needed.

5.4 SUMMARY

FE analysis of both bolted and welded single angles was conducted to further investigate the shear lag effect on the tensile capacity of HSS angles. FE models of all test specimens were developed. The FE analysis results of the test specimens were generally in good agreement with the test results. Subsequently, the validated FE models were used to conduct a parametric study for a more comprehensive investigation on the shear lag effect of HSS bolted single angles. An enhanced range of parameters, including steel grade, connection length, and out-of-plane eccentricity was included. In particular, the range of steel grade was extended to S960. The results of the parametric study showed that the shear lag effect became more severe when a higher steel grade was used for the angles with equal or short leg connections. However, for the angles with long leg connections, the shear lag effect was insignificant. Generally, the efficiencies of the angles increased with increasing connection length or decreasing out-of-plane eccentricity. Furthermore, the $1-\bar{x}/L$ rule (U_{RULE}) was verified against the FE predictions of the angles (U_{FEM}) in the parametric study. A good agreement was found between U_{RULE} and U_{FEM} for angles made of S275 steel irrespective of the connection type. In addition, the $1-\bar{x}/L$ rule was able to provide conservative predictions of the efficiencies of the HSS (S690 and S960 steel) angles with long leg connections compared with the FE analysis. However, for the HSS angles with equal or short leg connections, the predictions of efficiency by the $1-\bar{x}/L$ rule were found un-conservative in different extents. The largest overestimation could reach 20%. Thus, a modified equation based on $1-\bar{x}/L$ rule was required to predict the tensile capacity of HSS bolted single angles with short leg connections.

Table 5.1 True stress-strain data used in the model of S690, S275 and S960 steels

S690		S275	
True plastic strain	True stress (MPa)	True plastic strain	True stress (MPa)
0	761	0	292
0.019	779.9	0.015	298.6
0.025	796.5	0.021	335.9
0.033	810.1	0.029	367.7
0.045	830.2	0.076	470.5
0.058	843.6	0.103	504.1
0.915	1168.0	0.147	533.0
		0.183	554.3
		0.946	767.0

S960	
True plastic strain	True stress (MPa)
0	1002.5
0.015	1016.3
0.044	1089.8
0.747	1328.0

Table 5.2 Numerical results of the bolted angle specimens

Specimen	Ultimate load P_{Test} (kN)	FEM load P_{FEM} (kN)	P_{Test}/P_{FEM}
A1-60L	632	664	0.95
A1-75L	656	677	0.97
A1-90L	660	679	0.97
A1-75S	542	580	0.93
A2-60S	590	611	0.97
A2-75S	613	637	0.96
A2-90S	625	658	0.95
B1-75L	395	360	1.10
B2-75S	311	408	0.76

Table 5.3 Numerical results of the welded angle specimens

Specimen	Ultimate load P_{Test} (kN)	FEM load P_{FEM} (kN)	P_{Test}/P_{FEM}
C1-220L	796	791	1.01
C1-300L	839	832	1.01
C1-380L	850	826	1.03
C1-300S	748	725	1.03
C2-220S	836	843	0.99
C2-300S	823	835	0.99
C2-380S	925	930	0.99
D1-300L	488	480	1.02
D2-300S	511	531	0.96

Table 5.4 Results of parametric study

Designation	Section size (mm)	Steel grade	Bolt number	FEM load (kN)	FEM efficiency U_{FEM}	$1-\bar{x}/L$ (U_{Rule})	U_{FEM}/U_{Rule}
M1-L-3	75 x 50 x 8	S275	3	314	0.95	0.91	1.04
M1-L-4	75 x 50 x 8	S275	4	316	0.95	0.94	1.01
M1-L-5	75 x 50 x 8	S275	5	316	0.95	0.96	1.00
M1-E-3	75 x 75 x 8	S275	3	362	0.85	0.86	1.00
M1-E-4	75 x 75 x 8	S275	4	380	0.90	0.90	0.99
M1-E-5	75 x 75 x 8	S275	5	382	0.90	0.93	0.97
M1-S-3	75 x 100 x 8	S275	3	390	0.76	0.79	0.96
M1-S-4	75 x 100 x 8	S275	4	424	0.82	0.86	0.96
M1-S-5	75 x 100 x 8	S275	5	440	0.85	0.90	0.95
M2-L-3	75 x 50 x 8	S690	3	565	0.99	0.91	1.08
M2-L-4	75 x 50 x 8	S690	4	570	1.00	0.94	1.06
M2-L-5	75 x 50 x 8	S690	5	570	1.00	0.96	1.04
M2-E-3	75 x 75 x 8	S690	3	590	0.81	0.86	0.94
M2-E-4	75 x 75 x 8	S690	4	635	0.87	0.90	0.96
M2-E-5	75 x 75 x 8	S690	5	661	0.90	0.93	0.98
M2-S-3	75 x 100 x 8	S690	3	610	0.69	0.79	0.87
M2-S-4	75 x 100 x 8	S690	4	655	0.74	0.86	0.86
M2-S-5	75 x 100 x 8	S690	5	687	0.77	0.90	0.86
M3-L-3	75 x 50 x 8	S960	3	708	0.95	0.91	1.04
M3-L-4	75 x 50 x 8	S960	4	737	0.99	0.94	1.05
M3-L-5	75 x 50 x 8	S960	5	742	0.99	0.96	1.04
M3-E-3	75 x 75 x 8	S960	3	744	0.78	0.86	0.91
M3-E-4	75 x 75 x 8	S960	4	797	0.84	0.90	0.92

Table 5.4 Results of parametric study (Cont'd)

Designation	Section size (mm)	Steel grade	Bolt number	FEM load (kN)	FEM efficiency U_{FEM}	$1-\bar{x}/L$ (U_{Rule})	U_{FEM} $/U_{Rule}$
M3-E-5	75 x 75 x 8	S960	5	834	0.87	0.93	0.94
M3-S-3	75 x 100 x 8	S960	3	777	0.67	0.79	0.85
M3-S-4	75 x 100 x 8	S960	4	833	0.72	0.86	0.83
M3-S-5	75 x 100 x 8	S960	5	873	0.75	0.90	0.84
A1	100 x 100 x 8	S690	3	741	0.71	0.81	0.87
A2	100 x 100 x 8	S690	4	798	0.76	0.88	0.87
A3	100 x 100 x 8	S690	5	843	0.80	0.91	0.89
A4	75 x 75 x 6	S690	4	474	0.85	0.91	0.94
A5	75 x 75 x 10	S690	4	487	0.88	0.90	0.97
A6	75 x 100 x 6	S690	4	786	0.72	0.86	0.83
A7	75 x 100 x 10	S690	4	810	0.74	0.86	0.86
A8	100 x 100 x 8	S275	4	530	0.87	0.91	0.96
A9	100 x 100 x 8	S960	4	1077	0.79	0.91	0.87
A10	75 x 125 x 8	S275	5	482	0.79	0.86	0.92
A11	75 x 125 x 8	S690	5	711	0.68	0.86	0.79
A12	75 x 125 x 8	S960	5	908	0.66	0.86	0.77

Notes: In the group of designation like "M1-L-3", "M1" refers to material of S275; "M2" refers to material of S690; "M3" refers to material S960. "L" refers to long leg connection; "E" refers to equal leg connection; "S" refers to short leg connection. And the number "3", "4" and "5" refers to the number of bolts. In other comparison groups, no special designations are used.

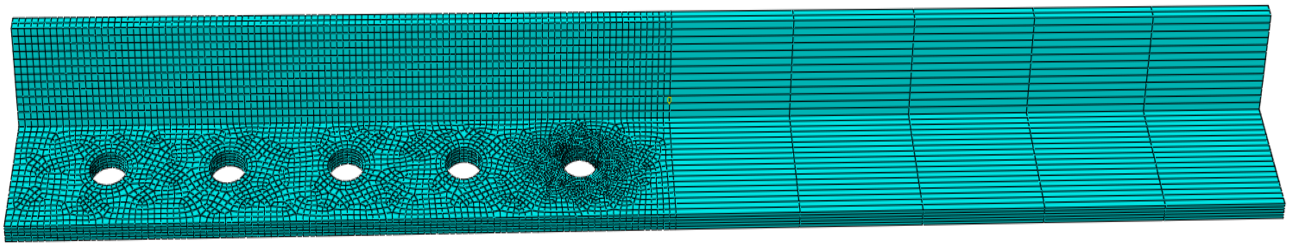

Angle

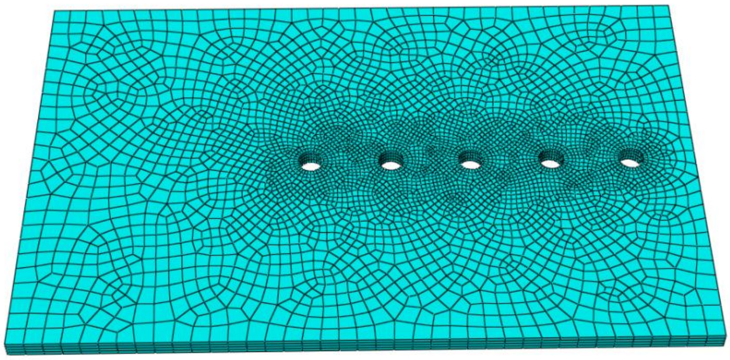

Gusset plate

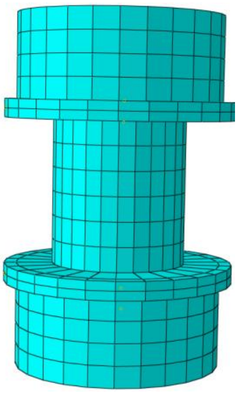

Bolt

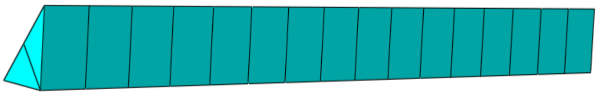

Weld

Figure 5.1 Models of each component of the specimen

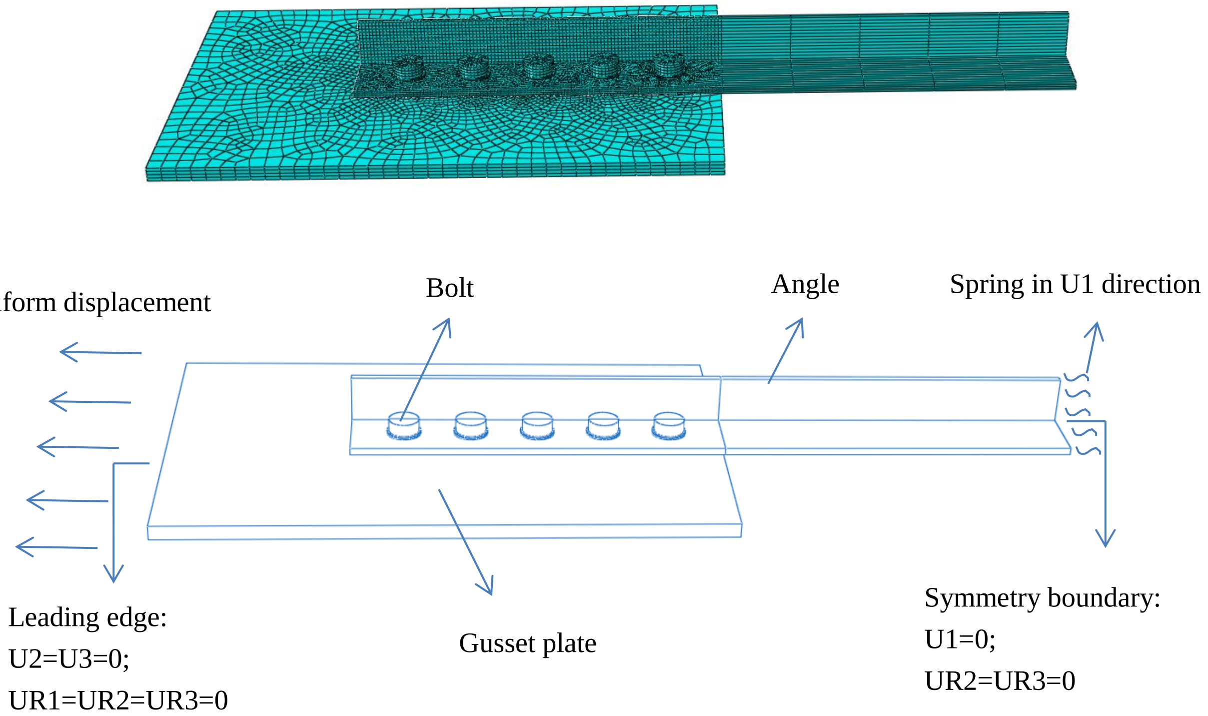

Figure 5.2 Typical finite element model of the bolted angle specimen

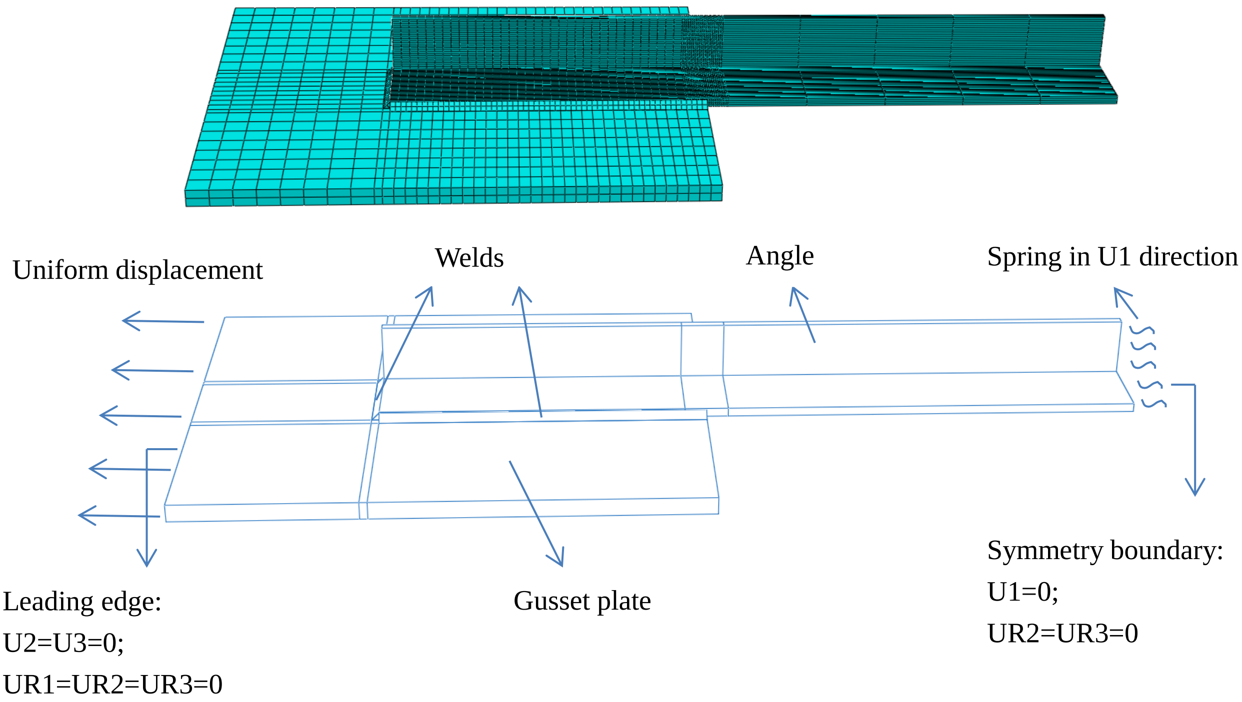

Figure 5.3 Typical finite element model of the welded angle specimen

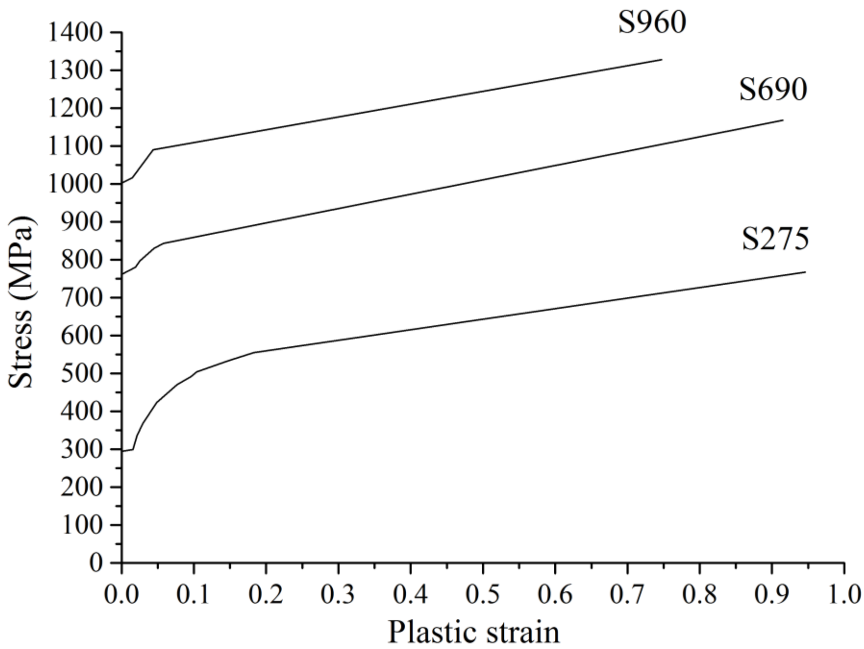

Figure 5.4 True stress-strain curves of S690 and S275 steel

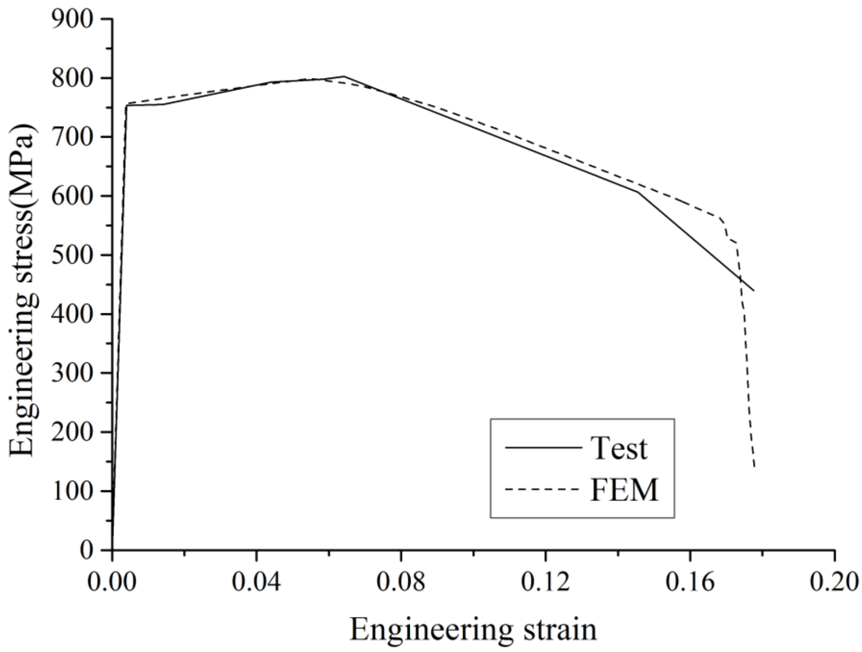

Figure 5.5 Validation of material model of S690 steel

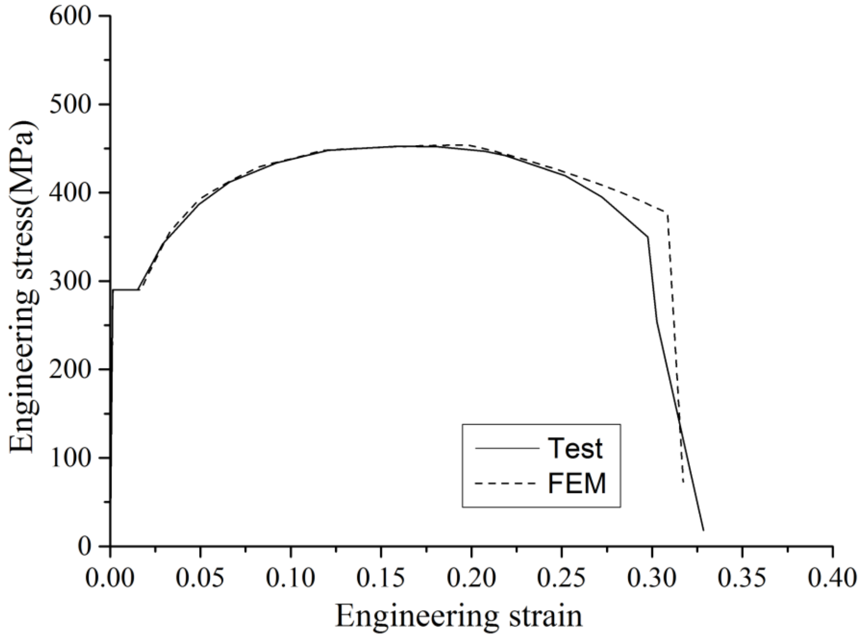

Figure 5.6 Validation of material model of S275 steel

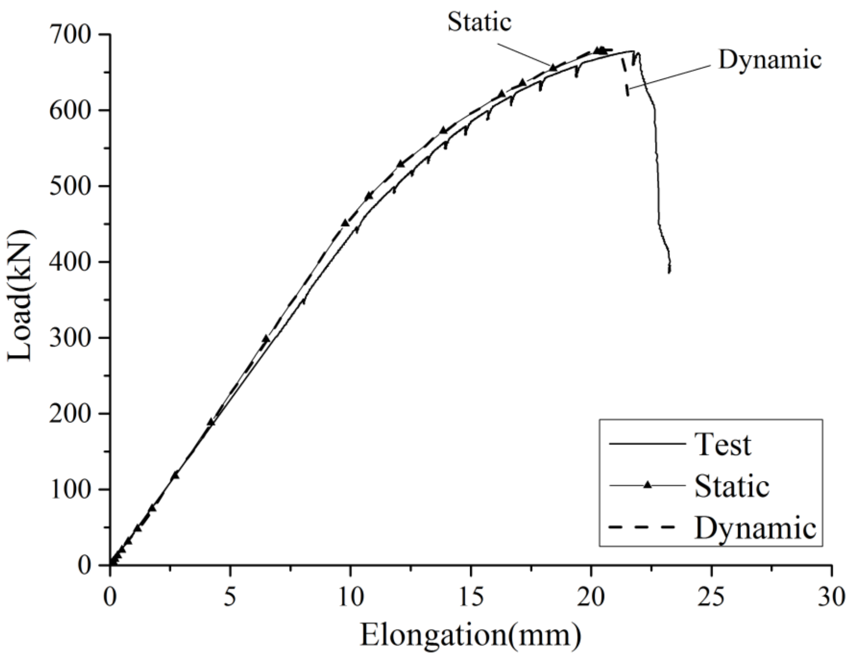

Figure 5.7 Comparison of load-elongation curves using dynamic and static method

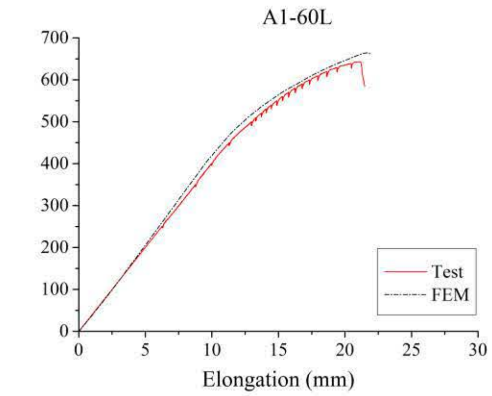
A1-60L
Elongation (mm)
Test
FEM

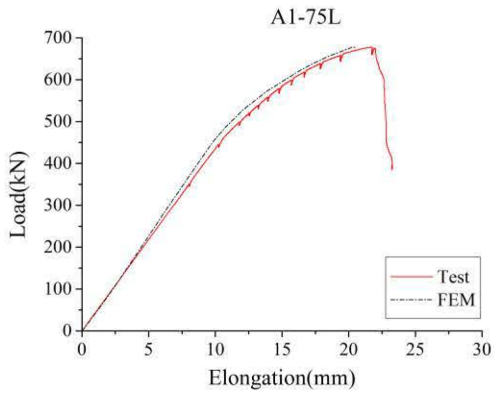
A1-75L
Load(kN)
Elongation(mm)
Test
FEM

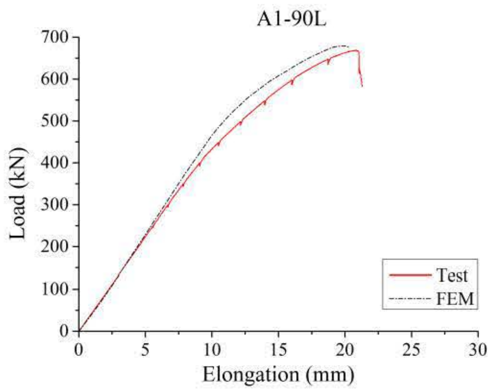
A1-90L
Load (kN)
Elongation (mm)
Test
FEM

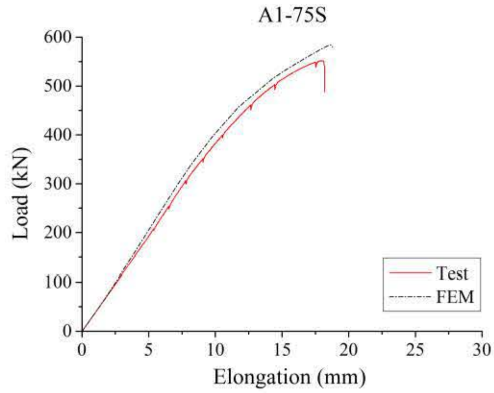
A1-75S
Load (kN)
Elongation (mm)
Test
FEM

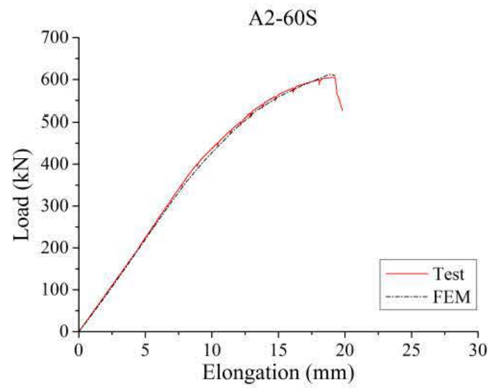
A2-60S
Load (kN)
Elongation (mm)
Test
FEM

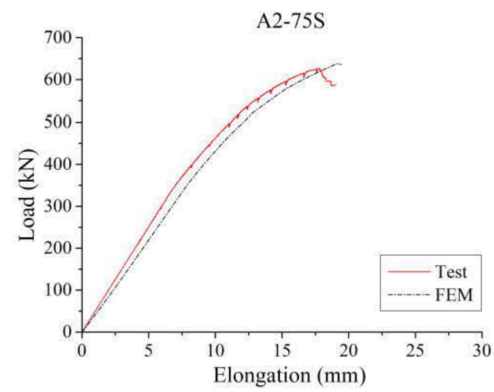
A2-75S
Load (kN)
Elongation (mm)
Test
FEM

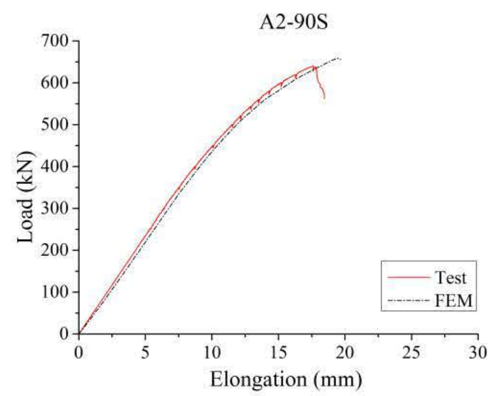
A2-90S
Load (kN)
Elongation (mm)
Test
FEM

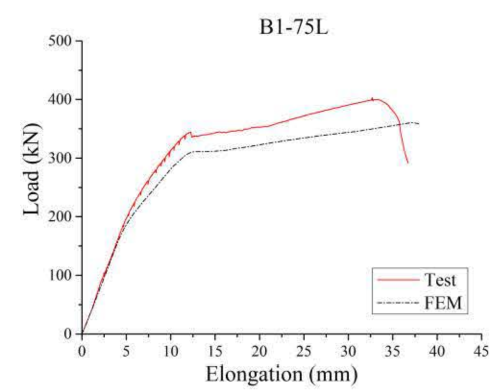
B1-75L
Load (kN)
Elongation (mm)
Test
FEM

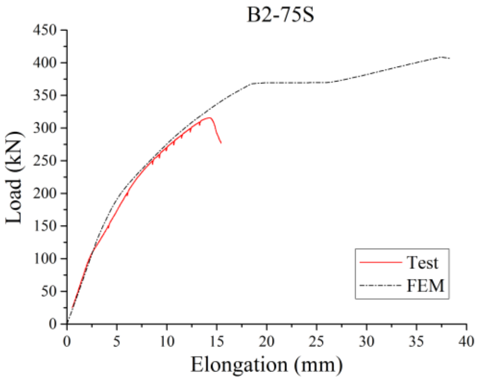

Figure 5.8 Comparison of FEM and test load-elongtion curves of bolted angle specimens

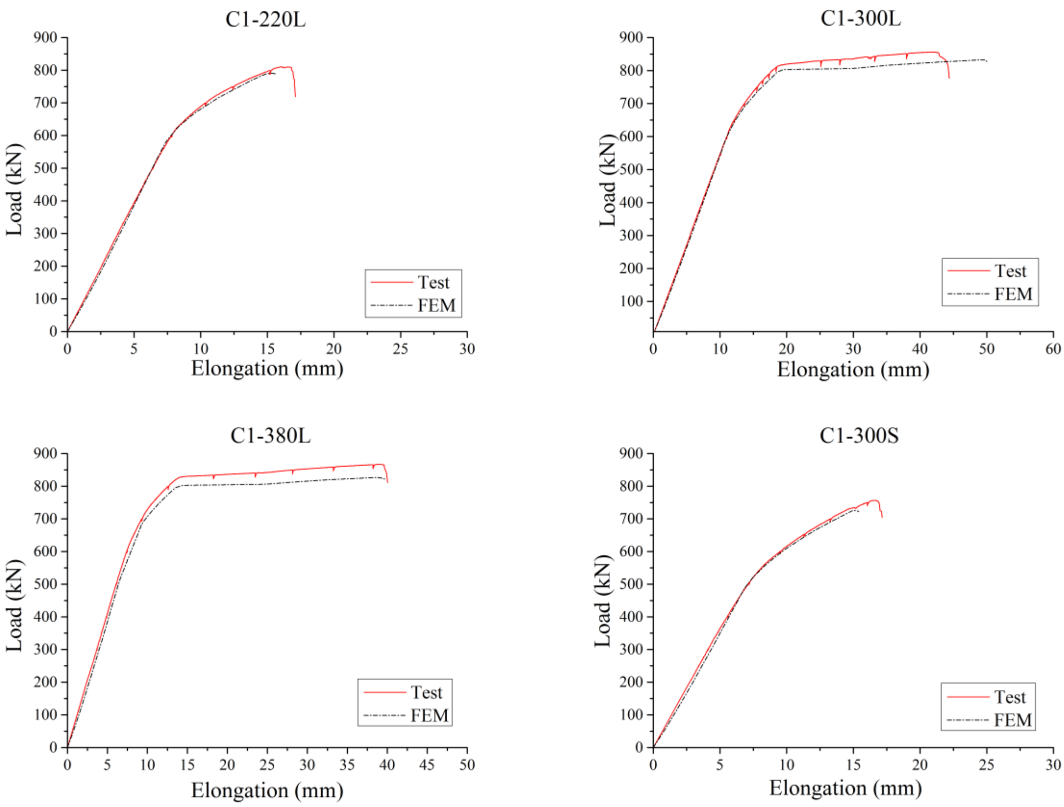

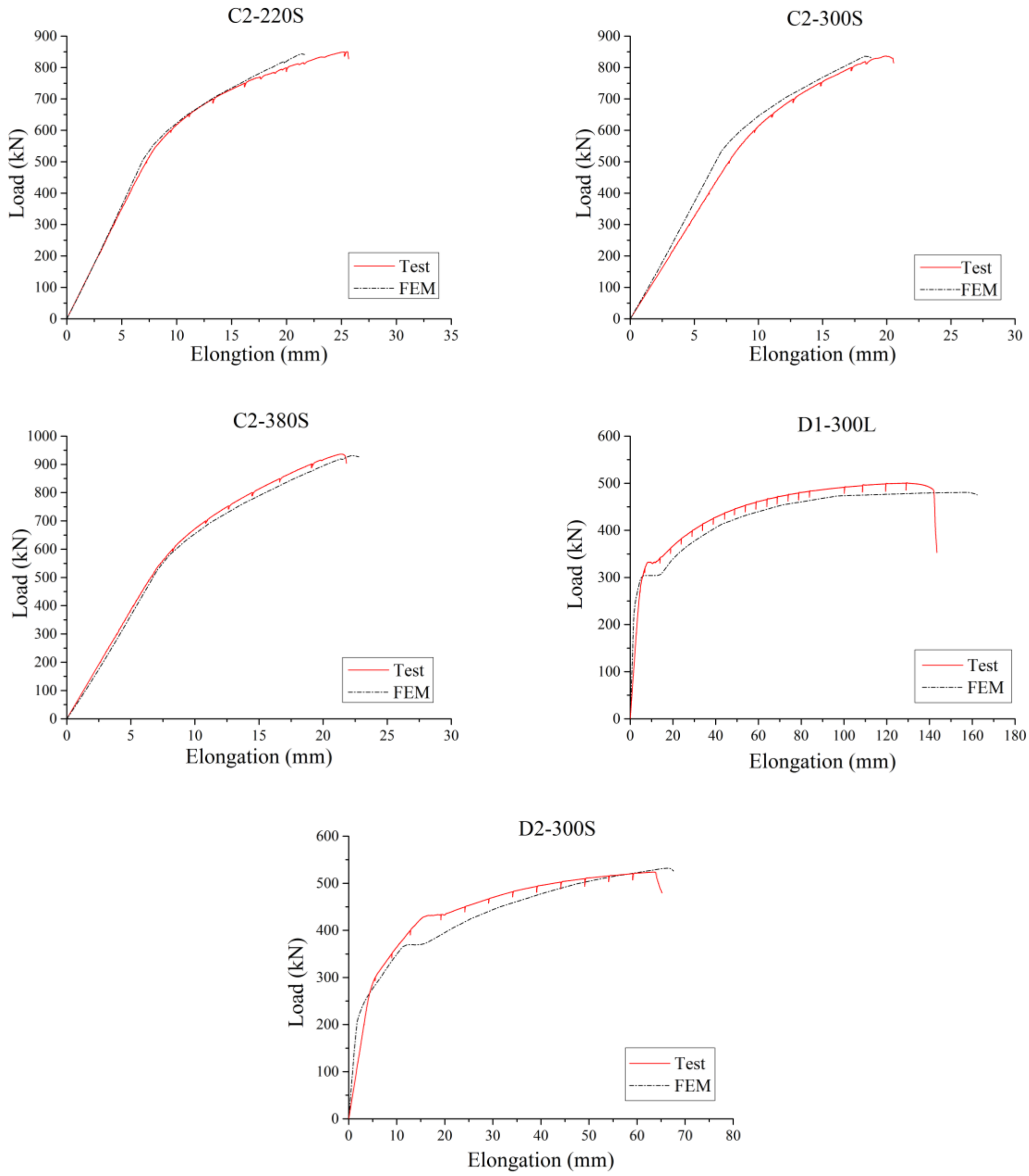

Figure 5.9 Comparison of FEM and test load-elongtion curves of welded angle specimens

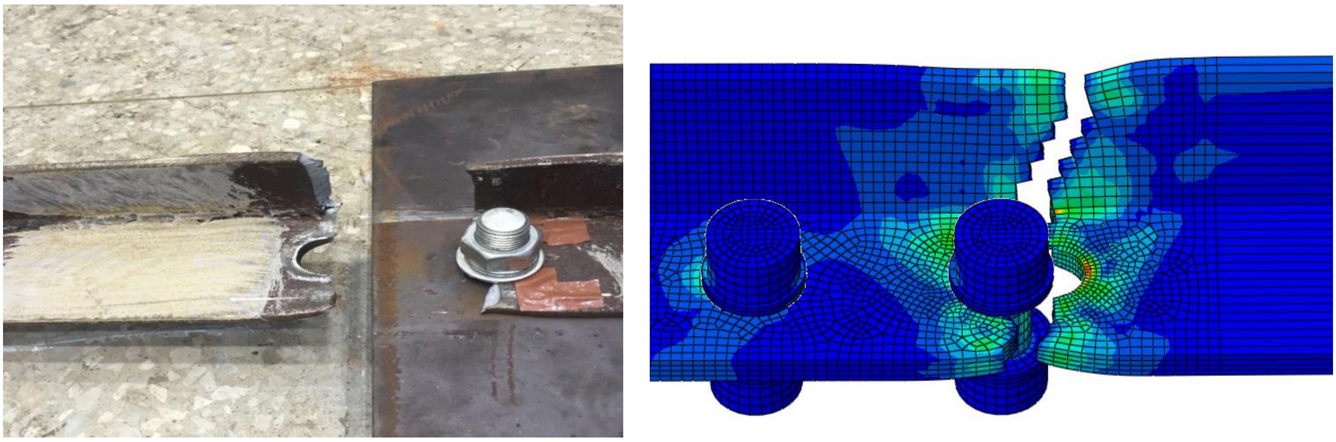

Figure 5.10 Comparison of test and FEM failure mode of the bolted angle specimens

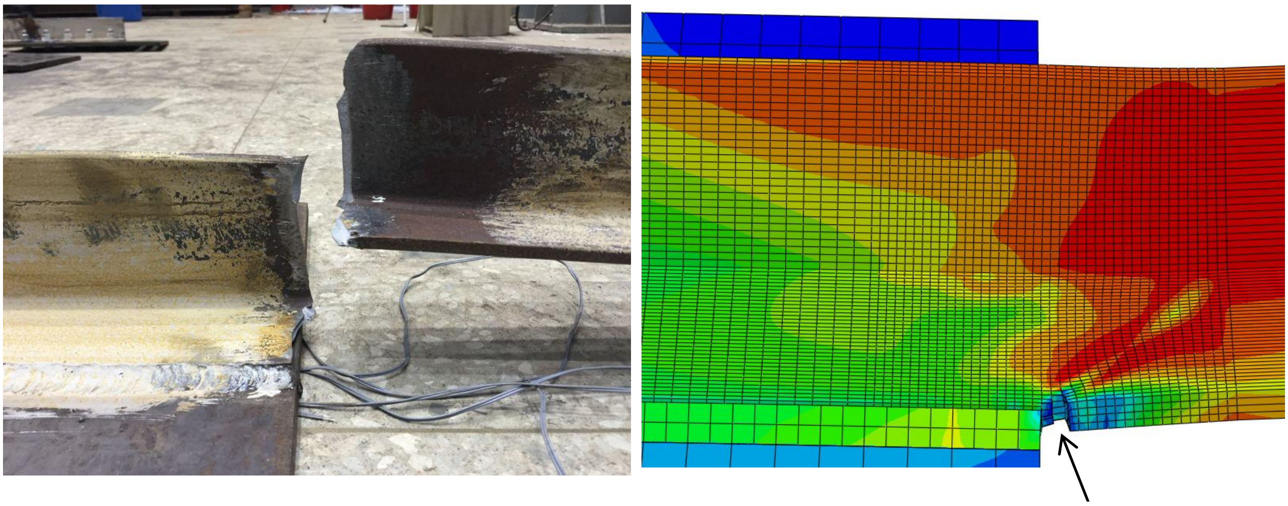

Crack initiated at critical section

Figure 5.11 Comparison of test and FEM failure mode of welded angle specimens

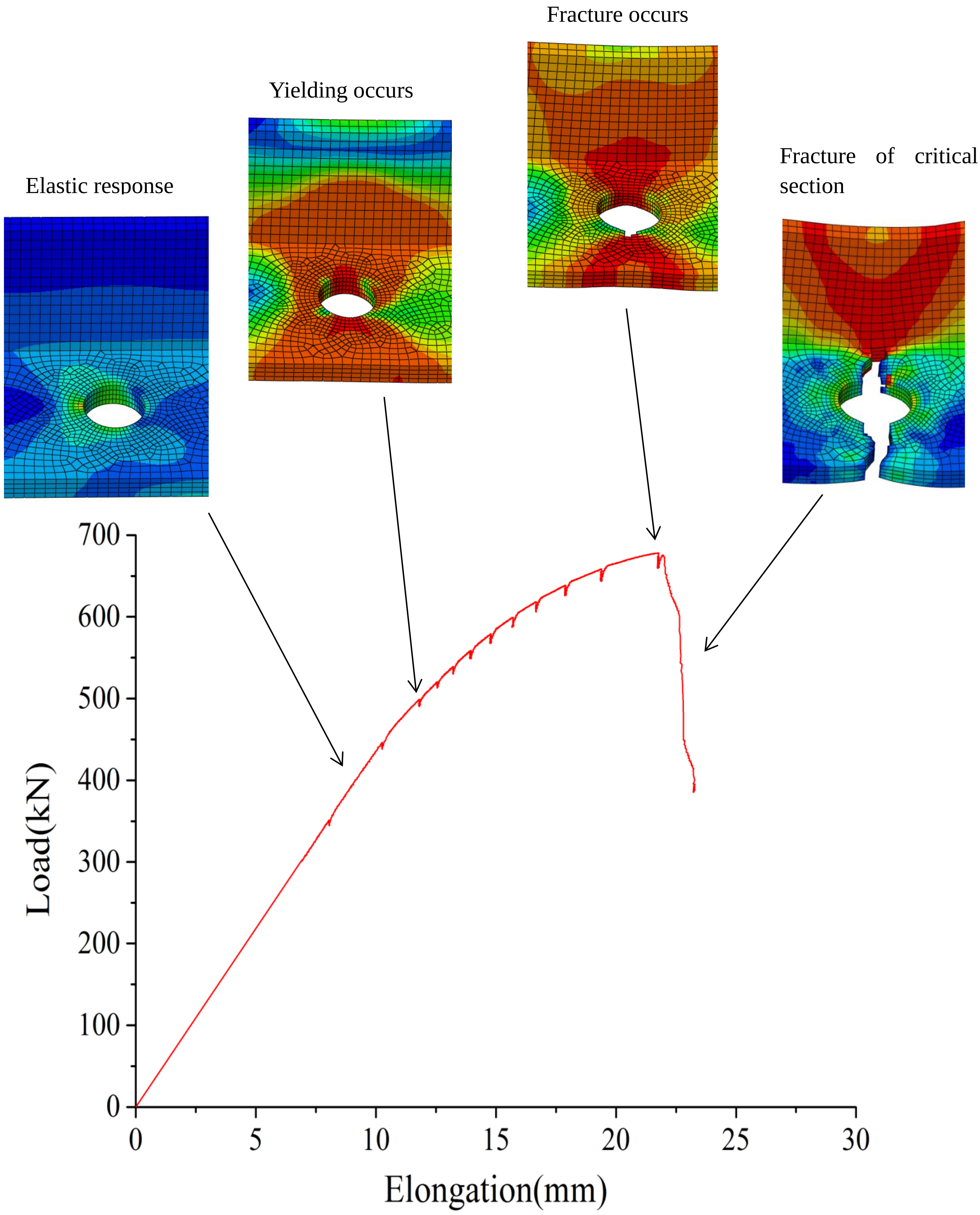

Figure 5.12 Typical fracture process of bolted angle specimens

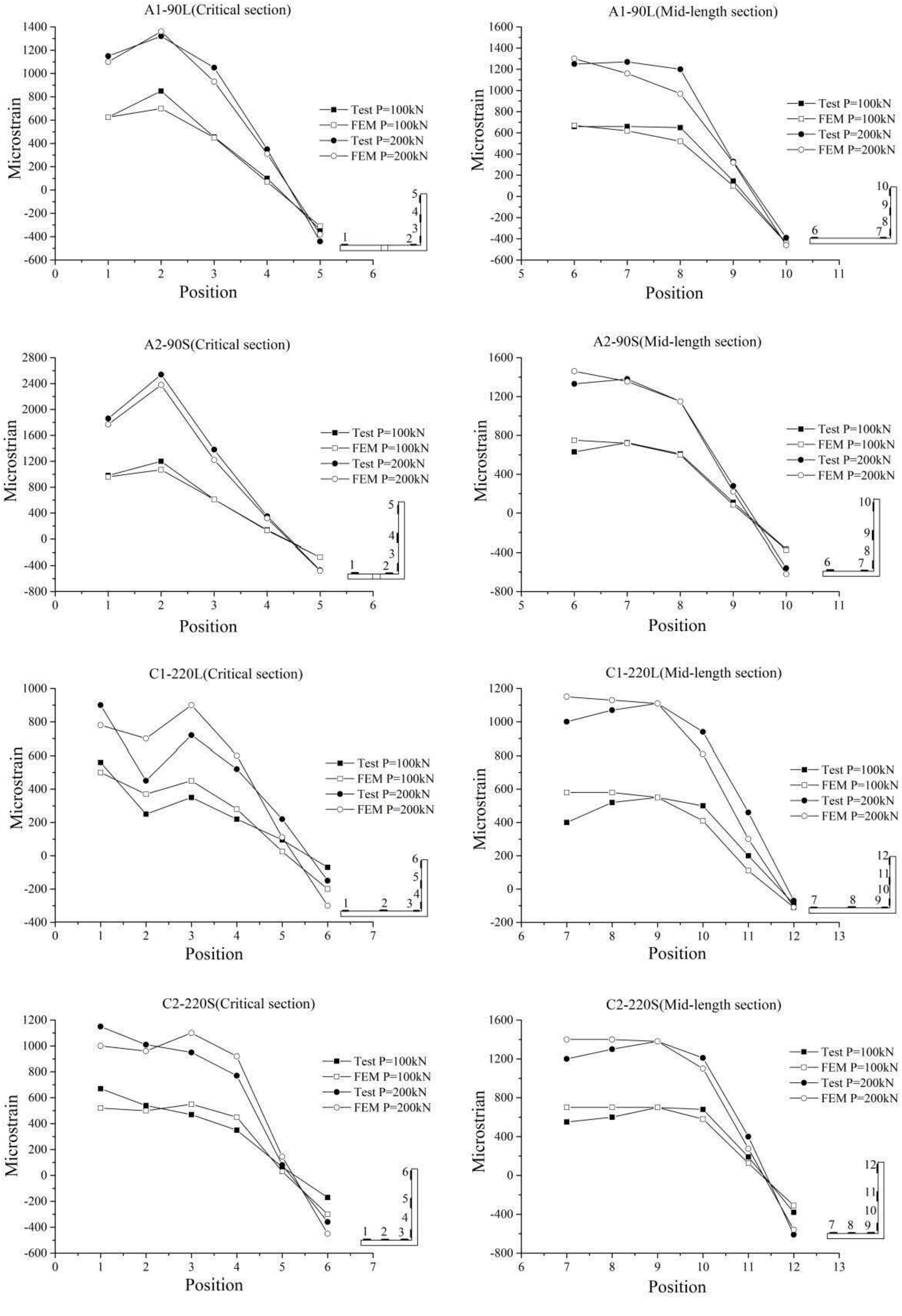

Figure 5.13 Typical comparisons of test and FEM strain distributions

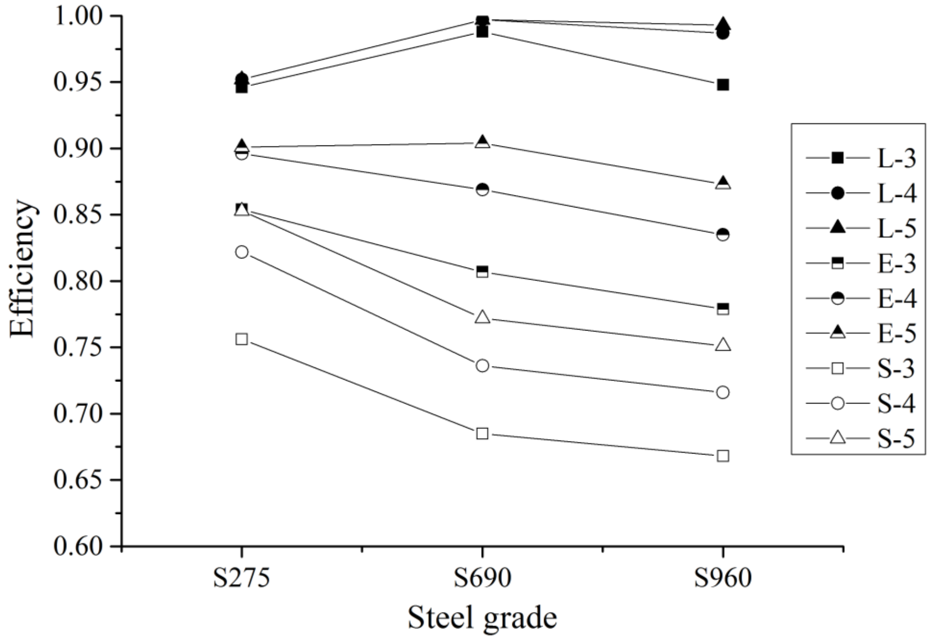

Figure 5.14 Comparison of specimens made of different steel grades

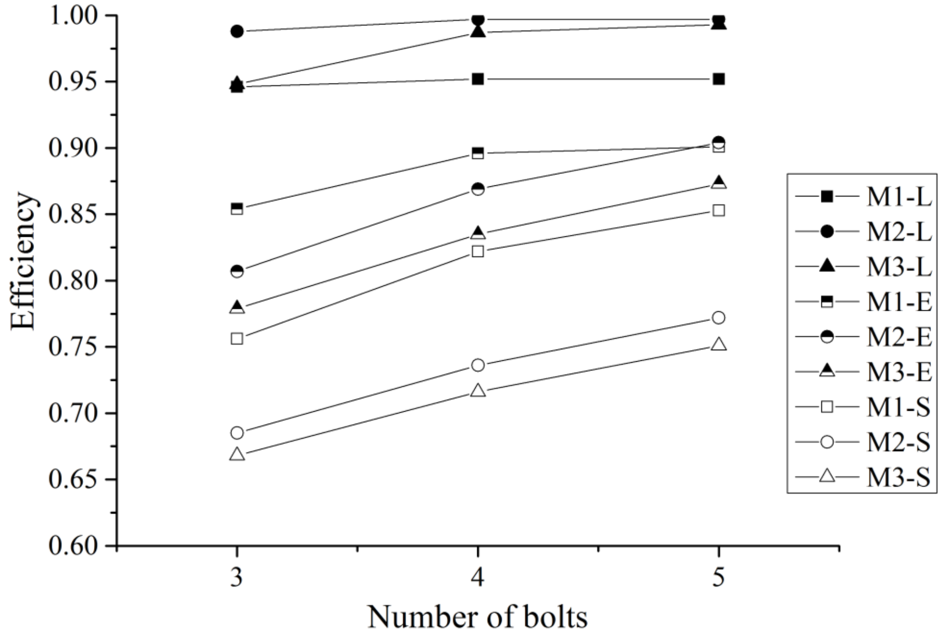

Figure 5.15 Comparison of specimens with different connection length

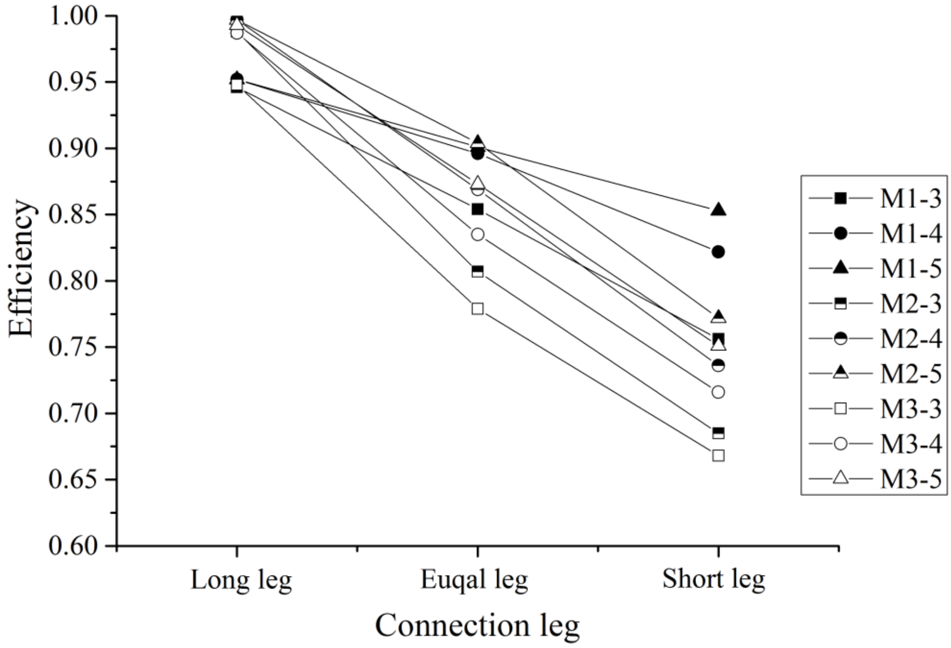

Figure 5.16 Comparison of specimens with different out-of-plane eccentricity

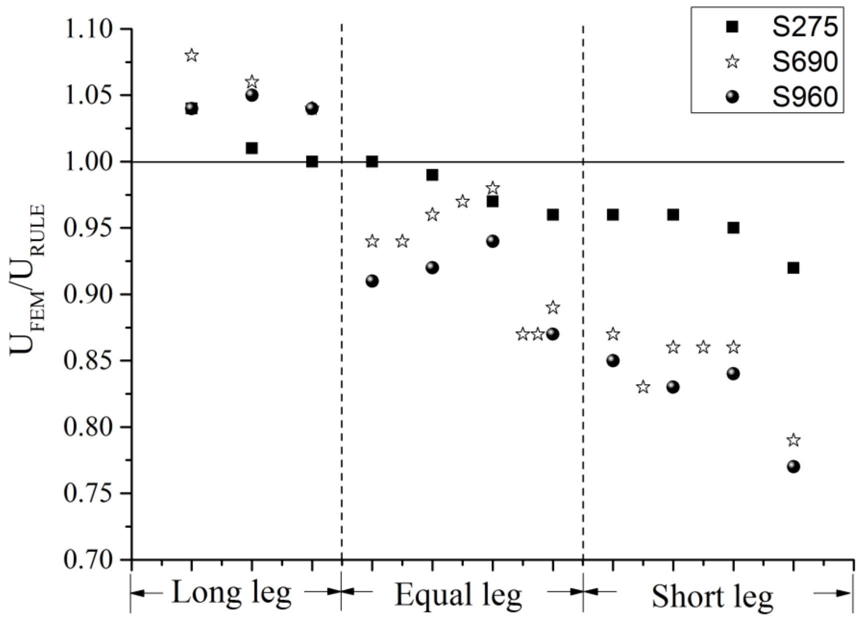

Figure 5.17 Evaluations of $1 - \bar{x}/L$ rule

CHAPTER 6 DESIGN RECOMMENDATIONS

6.1 PROPOSED DESIGN EQUATION

As mentioned previously, the $1 - \bar{x}/L$ rule used in the present AISC steel design code (AISC, 2010) was able to provide good predictions of the shear lag effect of angles made of S275 steel and long leg connected angles made of S690 and S960 steels. By contrast, overestimation of up to 20% was found for equal and short leg connected angles made of S690 and S960 steels. Thus, a modified equation based on the $1 - \bar{x}/L$ rule was proposed to assess the shear lag effect of the angles connected by the short leg. The effect of steel grade was considered using a reduction factor (α_m), determined based on the parametric study result, and applied to the original equation as shown in Eqn. 6.1.

$$U = \alpha_m(1 - \bar{x}/L) \tag{6.1}$$

Where U = net section efficiency

α_m = reduction factor

$\bar{x}$ = out-of-plane eccentricity

L = connection length

According to Chesson and Munse (1953), the $1 - \bar{x}/L$ rule was proposed by ensuring that the majority of the 1000 test data fell within the 10% scatter bands of Eqn. 2.2. Therefore, a similar approach was adopted to determine the reduction factor based on the 10% scatter bands of the numerical data for Eqn. 6.1. Thus, the reduction factor was determined to be 0.88. The proposed equation is expressed as Eqn. 6.2. The comparison of the efficiency evaluated based on the numerical data and that of the proposed equation is illustrated in Figure 6.1. The figure indicates that most of the numerical data based on either S690 steel or S960 steel fell within the 10% scatter bands of Eqn. 6.2. Notably, the data of angles made of S275 steel and long leg connected angles made of S690 and S960 steels are not included in the figure.

$$U = 0.88(1 - \bar{x}/L) \quad (6.2)$$

The ratio of FEM efficiencies to the predicted efficiencies by Eqn. 6.2 ranged from 0.88 to 1.11 with a mean value of 1.00 and a coefficient of variation of 0.06. Therefore, Eqn. 6.2 can provide a reasonable prediction of the numerical data.

6.2 EVALUATION OF THE PROPOSED EQUATION

The proposed equation to predict the efficiency of equal and leg connected angles made of S690 and S960 steels was verified by the test data. The comparisons are plotted in Figure 6.2. The ratios of test efficiency to predicted efficiency by Eqn. 6.2 range from 0.92 to 0.98 with a mean value of 0.94 and a coefficient of variation of 0.02. Although the proposed equation still provides un-conservative predictions, the extent of overestimation is within a reasonable range (10%). Furthermore, compared with the ratios of test to predicted efficiencies by the $1 - \bar{x}/L$ rule that have a mean value of 0.82 and a coefficient of variation of 0.01, the proposed equation provides a much better prediction of efficiency of HSS angles connected by a short leg.

In addition, the proposed equation was developed based on the numerical data from the parametric study and verified only by four test data of angle specimens made of S690 steel. No test data of the specimens made of S960 steel were available for verification. Thus, to further confirm the validity of Eqn. 6.2, conducting more tensile tests of bolted HSS angles connected by a short leg made of S690 and S960 steels is recommended. Moreover, in current study, only one reduction factor is employed for two different steel grades (S690 and S960 steels). It is recommended that in the future study, different reduction factors for different steel grades can be determined by more tests

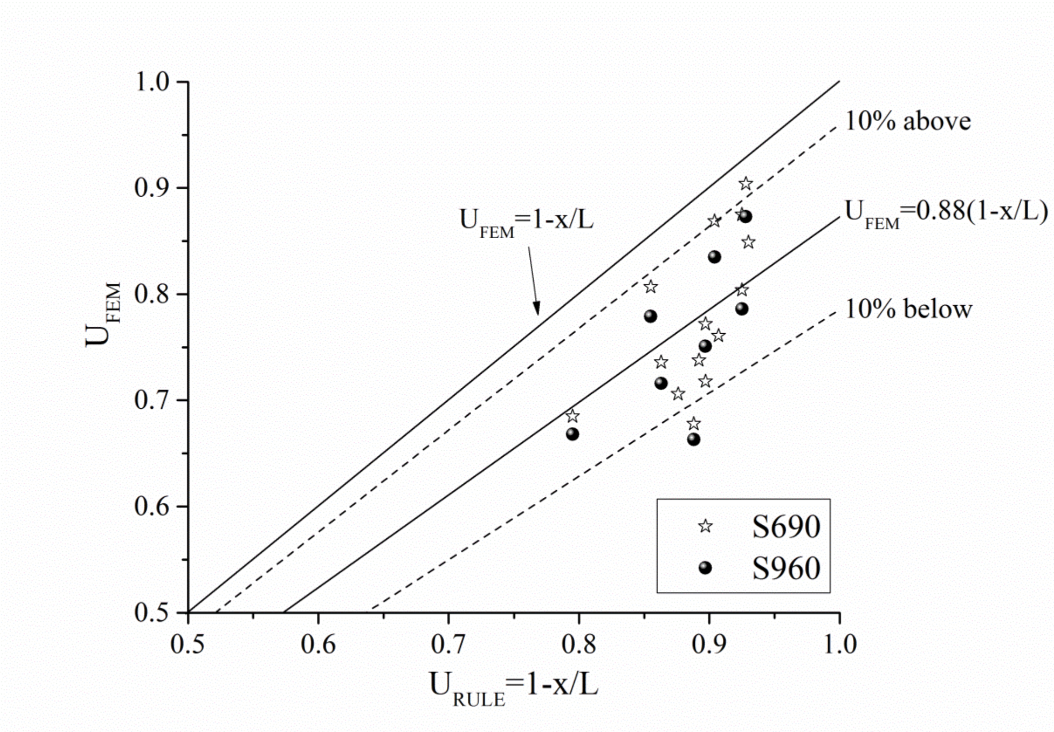

Figure 6.1 Comparison of numerical data and proposed equation

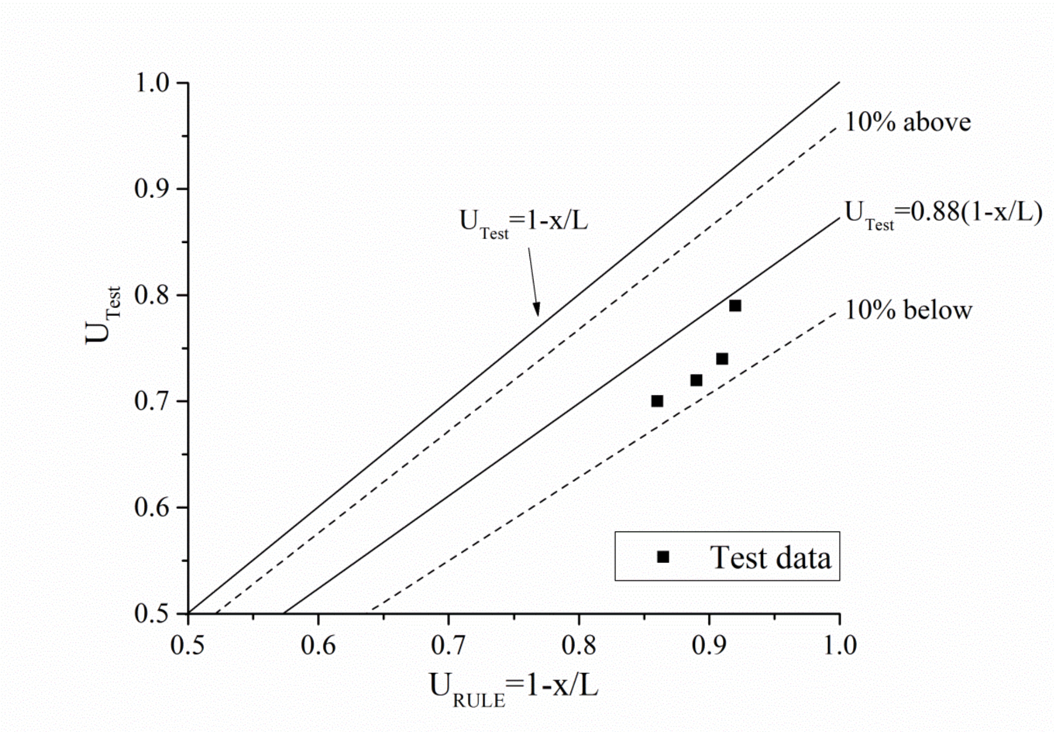

Figure 6.2 Comparison of test data and proposed equation

CHAPHTER 7 SUMMARY AND CONCLUSIONS

7.1 SUMMARY AND CONCLUSIONS

Recently, HSS have gained increasing popularity in the construction industry given their beneficial effects. One of the concerns about widely using HSS in construction is that HSS possess much lower ductility than that of NS. In particular, the reduced ductility of HSS materials may have a significant effect on the tensile strength and behaviour of angle sections, which are usually governed by the shear lag effect. Although many studies on the shear lag effect of bolted and welded single angles have been conducted, none of these studies focused on HSS tension members. In addition, all the current design equations, including the effect of shear lag, were established on the basis of the test data of NS tension members; thus, they may not be applicable to HSS tension members.

The primary goal of this thesis is to examine the effect of steel grade (ductility of steel) on the shear lag effect of single angles and to verify the applicability of the widely used equation, $1 - \bar{x}/L$ rule for assessing the shear lag effect, to HSS tension angle members. A total of 18 full-scale bolted and welded single angles, including 14 HSS specimens, were tested in the experimental programme. FE models were also established for further investigation. A numerical parametric study with an expanded range of parameters was conducted using the validated FE models. A design equation based on the $1 - \bar{x}/L$ rule was proposed. The new equation provides a more accurate prediction of the test results than the $1 - \bar{x}/L$ rule. Based on the experimental and numerical results, the main conclusions of this study are drawn as follows:

1. Steel grade did not evidently affect the shear lag effect for bolted and welded angle specimens with a long leg connection. However, for the angle specimens with a short leg connection, the shear lag effect became more severe with higher steel grade (S690 and

S960).

2. The shear lag effect of HSS single angles was less significant as the connection length increased. For welded angles with long leg connections and relatively long connection length, full section capacity was achieved.

3. The shear lag effect of HSS single angles was significantly affected by out-of-plane eccentricity. The test efficiencies decreased considerably as out-of-plane eccentricity increased.

4. The $1 - \bar{x}/L$ rule could provide a good prediction of the efficiency of all HSS welded angles and HSS bolted angles with a long leg connection.

5. General overestimation of efficiency predicted by the $1 - \bar{x}/L$ rule was found for HSS bolted angles with equal and short leg connections.

6. Based on the parametric study, a new design equation to predict the efficiency (U) was proposed for HSS (S690 and S960 steel) bolted single angles with equal and short leg connections. A reduction factor of 0.88 was adopted to modify the $1 - \bar{x}/L$ rule to consider the effect of steel grade. The proposed equation provided more accurate predictions of efficiency than the $1 - \bar{x}/L$ rule.

7.2 RECOMMENDATIONS FOR FUTURE WORK

Although this research contributes to the basic understanding of the shear lag effect of HSS bolted and welded single angles, the test data remain limited. Additional experimental work is required to further verify and examine the effect of material ductility on the tensile capacity of angles. For example, the proposed equation was only verified by short leg connected angle specimens made of S690 steel. Test data on equal leg connections and specimens made of S960 steel are needed for further verification. In addition, the effect of steel grade was considered a constant reduction factor in the proposed equation. A more comprehensive reduction factor, which may be a function of the yield strength of material, should be further investigated.

References

American Institute of Steel Construction [AISC] (1986). Load and resistance factor design. Chicago.

American Institute of Steel Construction [AISC] (1993). Load and resistance factor design specifications for structural steel buildings. Chicago.

American Institute of Steel Construction [AISC] (1998). Load and resistance factor design specifications for structural steel buildings. Chicago.

American Institute of Steel Construction [AISC] (2010). Specification for structural steel buildings. *ANSI/AISC 360–10*, Chicago.

A.S.T.M. (2007). A709/709M, Standard Specification for Structural Steel for Bridges, West Conshohocken

A.S.T.M. (2000). A514/A514M, Standard Specification for High-Yield-Strength, Quenched and Tempered Alloyed Steel Plate, Suitbale for Welding, West Conshohocken

American Society for Testing and Materials [ASTM] (2015). Standard test methods and definitions for mechanical testing of steel products, ASTM standard A370-15. Philadelphia.

Ban, H. Y., Shi, G., Shi, Y. J., & Wang, Y. Q. (2011, July). Research progress on the mechanical property of high strength structural steels. In*Advanced Materials Research* (Vol. 250, pp. 640-648).

Bjorhovde, R. (2010). Performance and design issues for high strength steel in structures. *Advances in Structural Engineering*, *13*(3), 403-411.

British Standard Institution [BSI] (1969). The use of structure steel in building. BS449: Part 2. London.

British Standard Institution [BSI] (2000). Structure use of steel work in building, part 1. Code of practice for desing in simple and continuous construction: Hot-rolled sections. BS 5950:Part 1. London.

Brockenbrough, R. Inc. (1995). Effect of Yield-Tensile Ratio on Structural

Behaviour-High Performance Steels for Bridge Construction: ONR-AISI Agreement.

Cai, Y., & Young, B. (2014). Behavior of cold-formed stainless steel single shear bolted connections at elevated temperatures. Thin-Walled Structures,75, 63-75.

Cai, Y., & Young, B. (2014). Structural behavior of cold-formed stainless steel bolted connections. Thin-walled structures, 83, 147-156.

Canadian Standards Association (CSA) (1984). Limit states design of steel structures, *Standard CAN3-S16.1-M84,* Toronto, Ont.

Canadian Standards Association (CSA) (2009). Limit states design of steel structures, *Standard CAN/CSA-S16-09,* Toronto, Ont.

Chen, W.-F. (1997). *Handbook of structural engineering*: Crc Press.

Cheng, J. J. R., Kulak, G. L., & Khoo, H. A. (1998). Strength of slotted tubular tension members. Canadian Journal of Civil Engineering, 25(6), 982-991.

Chesson, E., & Munse, W. H. (1963). Riveted and bolted joints: Truss-type tensile connections. Journal of the Structural Division, 89(1), 67-106.

Commission of the European Communities [CEC] (1989). Eurocode 3. Design of steel structures.

Davis, R., & Boomslitter, G. (1934). Tensile tests of welded and riveted structural members. *Journal of the American Welding Society, 13*(4), 21-27.

Dexter, R. J., Alttstadt, S. A., & Gardner, C. A. (2002). *Strength and ductility of HPS70W tension members and tension flanges with holes*: American Iron and Steel Institute.

Dowling, N. E. (1993). Mechanical behavior of materials: engineering methods for deformation, fracture, and fatigue. Prentice hall.

Easterling, W. S., & Gonzales, L. (1993). Shear lag effects in steel tension members. *Engineering Journal, 3,* 77-89.

European Committee for Standardization [CEN] (1992). EN 1993-1-1. Eurocode 3: Design of steel structures: Part 1-1: General Rules and Rules for Buildings. Brussels

European Committee for Standardisation [CEN] (2005). EN 1993-1-8. Eurocode 3:

design of steel structures - Part 1-8: Design of joints. Brussels.

European Committee for Standardization [CEN] (2006). prEN 1993-1-12. Eurocode 3: design of steel structures - Part 1-12: additional rules for the extension of EN 1993 up to steel grades S 700. Brussels.

European Committee for Standardization [CEN] (2007). EN 1993-1-12. Eurocode 3: design of steel structures - Part 1-12: additional rules for the extension of EN 1993 up to steel grades S 700. Brussels.

Fang, C., Lam, A. C. C., & Yam, M. C. H.(2013). Influence of shear lag on ultimate tensile capacity of angles and tees. *Journal of Constructional Steel Research, 84*, 49-61.

Fukumoto, Y. (1996). New constructional steels and structural stability. *Engineering structures, 18*(10), 786-791.

Galambos, T. V., Hajjar, J., Earls, C., & Gross, J. L. (1997). *Required properties of high-performance steels*: National Institute of Standards and Technology, Building and Fire Research Laboratory.

Gibson, G., & Wake, B. (1942). An investigation of welded connections for angle tension members. *The Welding Journal*, 44.

Hibbit, H. D., Karlsson, B. I., & Sorensen, E. P. (2012). ABAQUS User Manual, Version 6.12. *Simulia, Providence, RI*.

Kim, H. J., & Yura, J. A. (1999). The effect of ultimate-to-yield ratio on the bearing strength of bolted connections. *Journal of Constructional Steel Research, 49*(3), 255-269.

Kouhi, J., & Kortesmaa, M. (1990). Strength Tests on Bolted Connections Using High-Strength Steels(HSS Steels) as a Base Material.

Kulak, G. L., & Wu, E. Y. (1997). Shear lag in bolted angle tension members. *Journal of Structural Engineering, 123*(9), 1144-1152.

Langenberg, P. (2008). Relation between design safety and Y/T ratio in application of welded high strength structural steels. In *Proceedings of International Symposium on Applications of High Strength Steels in Modern Constructions and Bridges-Relationship of Design Specifications, Safety and Y/T Ratio.*

Beijing (pp. 28-46).

Li Ling (2014). Behavior of steel beam-to-column connections in structural progressive collapse. Unpublished doctoral dissertation, Tongji University, Shanghai, China

Madugula, M. K., & Mohan, S. (1988). Angles in eccentric tension. *Journal of Structural Engineering, 114*(10), 2387-2396.

Može, P., & Beg, D. (2010). High strength steel tension splices with one or two bolts. *Journal of Constructional Steel Research, 66*(8), 1000-1010.

Može, P., & Beg, D. (2011). Investigation of high strength steel connections with several bolts in double shear. *Journal of Constructional Steel Research, 67*(3), 333-347.

Može, P., Beg, D., & Lopatič, J. (2007). Net cross-section design resistance and local ductility of elements made of high strength steel. *Journal of Constructional Steel Research, 63*(11), 1431-1441.

Nelson, H. (1953). Angles in tension. *British Constructional Steelwork Assoc. on Publication No 7, United Kingdom*, 8-18.

Orbison, J. G., Barth, K. E., & Bartels, P. A. (2002). Net section rupture in tension members with connection eccentricity. *Journal of Structural Engineering, 128*(8), 976-985.

Puthli, R., & Fleischer, O. (2001). Investigations on bolted connections for high strength steel members. *Journal of Constructional Steel Research, 57*(3), 313-326.

Raoul, J., & Günther, H.-P. (2005). *Use and application of high-performance steels for steel structures* (Vol. 8): Iabse.

Rasmussen, K., & Hancock, G. (1995). Tests of high strength steel columns. *Journal of Constructional Steel Research, 34*(1), 27-52.

Regan, P., & Salter, P. (1984). Tests on welded-angle tension members. *Structural Engineer, 62*, 25-30.

Sause, R., & Fahnestock, L. A. (2001). Strength and ductility of HPS-100W I-girders in negative flexure. *Journal of Bridge Engineering*, *6*(5), 316-323.

Sedlacek, G., & Müller, C. (2001). High strength steels in steel construction.*Niobium: Science & Technology, TMS: The Minerals, Metals & Materials Society, Orlando, Florida*.

Shi, G., & Ban, H. (2009). *Application and recent research advances of high strength steel structures.* Paper presented at the Proceedings of 2009 International Symposium on Steels for Infrastructure (ISSI 2009). Beijing.

Shi, G., Hu, F., & Shi, Y. (2014). Recent research advances of high strength steel structures and codification of design specification in China. *International Journal of Steel Structures, 14*(4), 873-887.

Sooi, T., Green, P., Sause, R., & Ricles, J. (1995). Stress-strain properties of high-performance steel and the implications for civil-structure design: ASM International, Materials Park, OH (United States).

Standards Australia. (2012). Steel structures. *AS 4100:1998/Amdt 1-2012*, Sydney.

Vasarhelyi, D. D., & Chiang, K. C. (1967). Coefficient of friction in joints of various steels. *Journal of the Structural Division*.

Willms, R. (2009). High strength steel for steel constructions. Nordic Steel.

Yan, S., & Young, B. (2011). Tests of single shear bolted connections of thin sheet steels at elevated temperatures—Part I: Steady state tests. Thin-Walled Structures, 49(10), 1320-1333.

Yan, S., & Young, B. (2012). Bearing factors for single shear bolted connections of thin sheet steels at elevated temperatures. Thin-Walled Structures, 52, 126-142.

Zhu, H., Yam, M. C. H., Lam, A. C. C., & Iu, V. (2009). The shear lag effects on welded steel single angle tension members. *Journal of Constructional Steel Research, 65*(5), 1171-1186.